EFFECTS OF STRAIN ON CARDIAC ELECTROPHYSIOLOGY AND MICROSTRUCTURE

by

Thomas Grant McNary

A dissertation submitted to the faculty of
The University of Utah
in partial fulfillment of the requirements for the degree of

Doctor of Philosophy

Department of Bioengineering

The University of Utah

December 2011

The University of Utah Graduate School

STATEMENT OF DISSERTATION APPROVAL

The dissertation of _____

has been approved by the following supervisory committee members:

_____ , Chair _____ Date Approved

_____ , Member _____ Date Approved

_____ , Member _____ Date Approved

_____ , Member _____ Date Approved

_____ , Member _____ Date Approved

and by _____ , Chair of the Department of _____

and by Charles A. Wight, Dean of The Graduate School.

ABSTRACT

Does strain induce changes in the electrical properties of the heart? Does strain affect the microstructure of cardiac myocytes? Others have considered these questions, but have been limited in their findings. I addressed the first question by measuring conduction velocity in papillary muscles in rest conditions and during applied strain. I also applied streptomycin, a nonselective stretch ion channel blocker, in the above conditions. In control, conduction velocity increased with strain before conduction block occurred. When streptomycin was applied conduction velocity peaked at a higher strain, but conduction block remained unchanged. Changes in electrical properties of papillary muscle allowed for changes in conduction velocity. Although streptomycin did not alter the strain at which conduction block occurred, it did shift the peak conduction velocity to a higher strain.

The second question was addressed by imaging isolated cardiac ventricular myocytes in varying degrees of contraction and strain using confocal microscopy. The length of transverse tubules (t-tubules), along with cross-section ellipticity, and orientation in myocytes were analyzed for cells in 16% contraction, rest, and 16% strain. Cells in contraction showed an increase in length of t-tubules with less elliptical cross-sections compared to cells in rest. Strained cells showed a decrease in length of t-tubules with less elliptical cross-sections than cells at rest. The orientation of t-tubule cross-sections changed in a similar manner when comparing contracted and strained cells with cells at rest. The transfer of strain to the t-tubule system supports the hypothesis that the motion

of t-tubules during contraction and stretch may constitute a mechanism for pumping extracellular fluid.

CONTENTS

LIST OF TABLES

LIST OF FIGURES

ACKNOWLEDGEMENTS

This work would not be as good as it is, if it were not for the help I've received from many people. I would like to thank Frank Sachse, who has helped me from the beginning, helping me to understand the work of science and learn the exactness needed for progress in such a field. I would also like to thank John Bridge and Kenneth Spitzer, who have also been mentors to me, for their patients and their guidance. Lastly, I would like to thank my family. They have not only been supportive, they have been encouraging, and I am deeply grateful for it.

1. INTRODUCTION

Strain Effects on Cardiac Tissues and Cells

Does stretch induce changes in the electrical properties of the heart? Can mechanical strain affect the microstructure of cardiac myocytes? These questions have been raised in many studies of cardiac physiology and pathophysiology. This dissertation is aimed at providing novel mechanistic insights into strain effects on cardiac structures and functions. I will devote this chapter to providing information necessary to understanding my experiments and methods. This will include a description of cellular and tissue anatomy of the heart, cardiac electrophysiology, and the influence of mechanical strain in heart disease.

Anatomy and Function of the Heart

The general anatomy and function of the heart are well established and explained in most physiology books[1-3]. The heart functions as a pump, pumping blood to the lungs and to the rest of the body. There are four chambers in the mammalian heart (Fig. 1.1), being divided into two atria and two ventricles on the left and right side. Blood returning from the body first enters the right atrium before entering the right ventricle. As the heart contracts the blood from the right ventricle is pumped to the lungs and on to the left side of the heart. The blood on the left side of the heart is pumped from the left atrium to the left ventricle, and then on to the rest of the body.

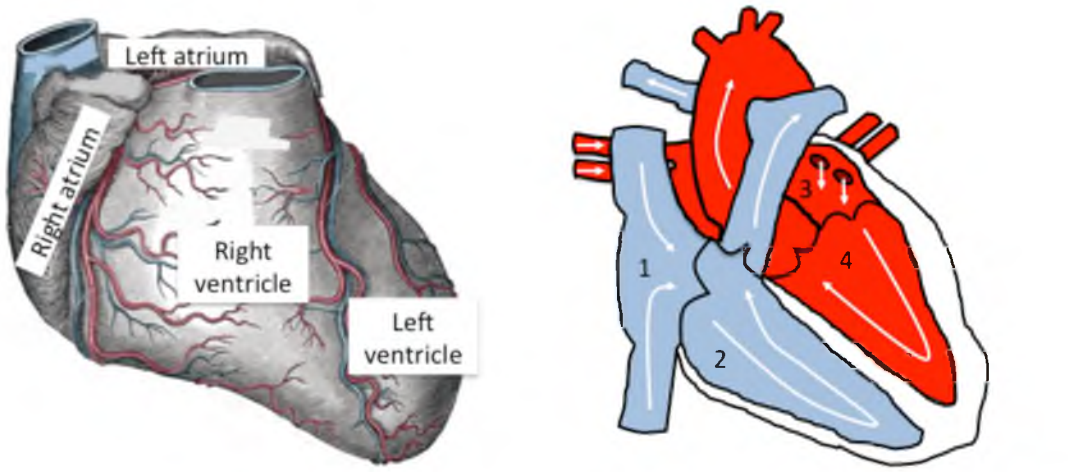

Figure 1.1: The human heart. The left image depicts the human heart as drawn in Gray's Anatomy of the Human Body, 1918. The image on the right depicts a cutaway view of the heart where the blue represents the unoxygenated blood and the red represents the oxygenated blood. The right atrium and ventricle are numbered 1 and 2, respectively, while the left atrium and ventricle are numbered 3 and 4, respectively.

To function as a pump, cardiac myocyte contraction in the atria and ventricles need to be coordinated, contracting in a coordinated manner. The signal to contract is initiated in the heart at the sinoatrial (SA) node, spreading over the atria. The atrioventricular (AV) node is the only electrical connection between the atria and the ventricles where the signal may pass from the atria to the ventricles. After the signal is delayed at the AV node, the signal propagates along the bundles of His and the Purkinje fibers, which make up the conduction system, to signal ventricular contraction.

Myocytes

Myocytes are both electrically and mechanically active. In the heart, myocytes are roughly 100 μm in length, 30 μm in width, and 15 μm in height; often being described as being "brick-shaped" although there are many irregularities in their shapes[6] (Fig. 1.2). Myocyte size is dependent on species as well as hemodynamic load[7, 8]. The major

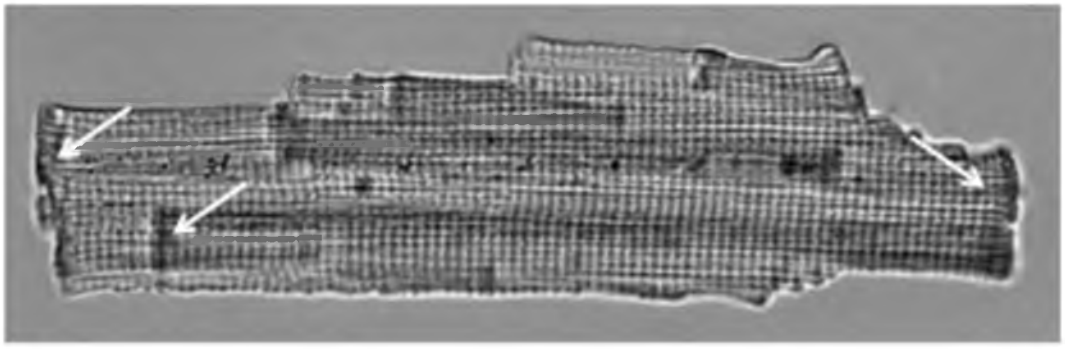

Figure 1.2: Transmission microscopic image of a dog ventricular myocyte. The vertical edges seen in this picture (marked by arrows) are locations where this cell may have connected to other myocytes via gap junctions. This image is courtesy of Dr. Kenneth Spitzer.

anatomical structures that affect how the myocyte functions mechanically and electrically include the sarcolemma, the system of transverse tubules (t-system), and the sarcomere as part of the cytoskeleton.

Sarcolemma

The sarcolemma comprises the outer membrane of the myocyte and the t-system, which is described later in this section. The sarcolemma is mainly made of phospholipids, cholesterol, glycolipids, and membrane proteins. The following description will focus on phospholipids and membrane proteins.

Phospholipids are amphipathic molecules, including a hydrophilic head group and a hydrophobic tail group. Due to these two chemical characteristics, the hydrophilic group is exposed to water and other charged molecules, while the hydrophobic lipids in a cell membrane are sandwiched in between the polar head groups. This arrangement of phospholipids prevents all polar molecules from crossing the membrane unless there is a pore, like an ion channel, to allow the polar molecules pass[4, 9]. For example, water would

not be able to cross the membrane if aquaporin, a protein that forms a membrane pore for water, were not present in the sarcolemma[10].

Here I consider four types of proteins most relevant to my work: ion channels, ion exchangers, ion pumps and gap junction channels. Each protein type is known to affect myocyte electrical activity. These types of proteins can be involved in other types of signaling, but the function of interest in this dissertation is focused on their effects on electrical activity.

Ion channels. There are myriad types of ion channels. Their function is to open or close a pore with different stimuli and allow or prevent ions to pass across the membrane. Commonly, channels exhibit selectivity to specific ions passing through their pore. Stimuli by which the channels may open or close include voltage, ligands, and strain. The duration of how long a channel remains in a specific state is variable depending on the type of channel.

Ion exchangers and pumps. Ion exchangers move one type of ion out of the cell while moving another type of ion into the cell. For example, the sodium-calcium (Na^+-Ca^{2+}) exchanger in the sarcolemma exchanges 3 Na^+ for 1 Ca^{2+} ion, depending on the electrochemical gradient of both ions[11]. Proteins that move ions against the concentration gradient at the direct expense of adenosine triphosphate (ATP) are ion pumps[12]. The sodium-potassium pump (Na^+-K^+ pump) pumps Na^+ out of and K^+ into the cell. Since this pump affects the concentration of Na^+, it indirectly affects the function of the Na^+-Ca^{2+} exchanger.

Gap junction channels. Gap junction channels are built of two hemi channels called connexons that are composed of connexins. There are many types of connexins found

through out the body of which three are prevalent in the heart: connexin 40 (Cx40), Cx43, and Cx45[13]. For a functional gap junction channel to exist between myocytes both cells need to contribute connexons, the connexons need to be linked, and the resulting channels need to be open. Properly formed gap junction channels act as open pores that connect the intracellular spaces of myocytes together, allowing ions and small molecules to pass between myocytes[14, 15]. Depending on the connexins involved in forming a gap junction channel the conductance of the channel will be higher or lower[13]. For instance if the gap junction channel is formed with Cx40-Cx40 linkage, the conductance is 162 pS. A Cx45-Cx45 gap junction channel, on the other hand, will have a conductance of 32 pS. Further description of gap junction channels' role in the electrical activity of the heart will be described later in this chapter.

Transverse Tubules

Transverse tubules (t-tubules) are invaginations in the sarcolemma, which are prevalent in some types of skeletal and cardiac myocytes. In cardiac myocytes, these invaginations significantly increase the surface to volume ratio[16], and allow electrical signaling to propagate deep into the cell. This is important because the high density of voltage activated calcium channels and Na^{+}-Ca^{2+} exchangers that line t-tubules are involved in excitation contraction coupling[17-19]. Electrical signals propagate much faster along the sarcolemma than calcium ions diffuse into the cell interior. Thus, voltage activated calcium channels within the t-tubules will allow a fast influx of calcium and synchronous triggering of adjacent calcium release unit in the sarcoplasmic reticulum. This would not be possible in the absence of t-tubules.

Cardiac t-tubules are only found in mammalian myocytes[17]. The distribution of t-tubules varies depending on the type of cardiac myocyte[17, 20, 21]. Commonly, myocytes from atria have sparsely developed t-systems, while ventricular cells typically have well-developed t-systems[20]. The t-system in rats is more of a network of tubules because of the many longitudinal components[22], while the t-system in rabbits is mainly composed of transverse components with few in the longitudinal direction[23].

Various studies have shown that there are many cytoskeletal proteins associated with t-tubules. This suggests mechanical stabilization of the t-system while the myocytes contract, during systole, and are stretched, during diastole[24, 25]. In addition to the proteins listed above, the inability of a study to electrically characterize nonselective stretch activated ion channels (SAC_{NS}) in adult cardiac myocytes has led some to believe that such channels are sequestered to the t-tubular membrane[26, 27]. This presupposes that mechanical deformation does occur in the t-tubules; otherwise these channels would not sense the mechanical signal. Thus, it is important to know if the t-tubule geometry changes during the cardiac cycle and if it does change, then to what extent. Such information would be important for understanding strain modulation of SAC_{NS} currents and subsequent myocyte electrophysiology.

Cytoskeleton

Proteins that make up the cytoskeleton maintain the shape of a myocyte and its ability to contract. The most notable proteins in the cytoskeleton of a cardiac myocyte are those directly associated with the contractile function, forming the sarcomere. These proteins are actin, myosin, troponin, and tropomyosin. Other cytoskeletal proteins are indirectly

involved in mechanical function by anchoring the contractile structures to the myocyte sarcolemma, which include actinin, vinculin, titin, and dystrophin.

The principal components needed for contraction are thin and thick filaments. Strands of actin, troponin, and tropomyosin make up thin filaments, which extend from the Z-disk (Fig. 1.3). Troponin and tropomyosin interact with the actin preventing myosin from binding to the actin at rest[28]. Though troponin and tropomyosin move to allow contraction to occur, such movement does not directly contribute to the movement of contraction. Thin filaments remain essentially the same length throughout the excitation contraction process. Myosin is the protein that provides the contractile force at the cost of ATP. Multiple myosin proteins aggregate to form thick filaments, which extend from the M-line (midline of the sarcomere) towards the Z-disk. The process by which contraction

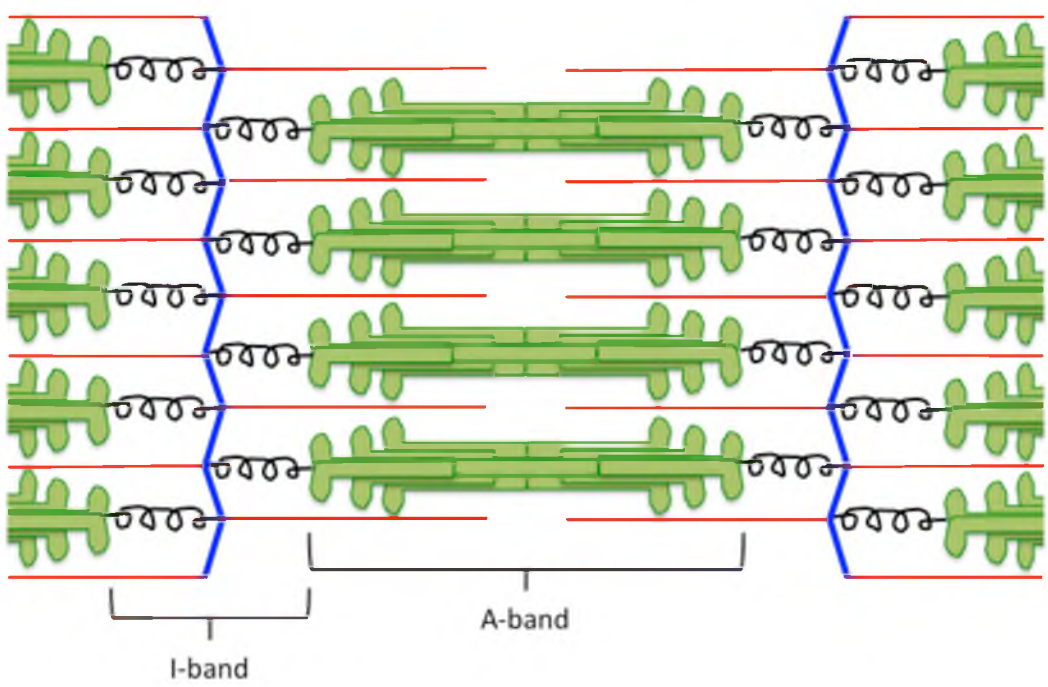

Figure 1.3: Schematic illustration depicting the architecture of a sarcomere. The Z-disk is represented in blue, the thin filaments in red, thick filaments in green, and titin in black. This is an adaptation from pages 962-963 of the textbook Molecular Biology of the Cell[4].

occurs will be explained in rudimentary detail later.

Anchor proteins are essential for transfer of contractile force within the cell to the sarcolemma. Dystrophin, for example, is integral in costamere formation, which anchors Z-disks to the sarcolemma. Actinin binds to actin, anchoring actin to the Z-disk and integrin receptors in sarcolemma. Titin is an elastomeric protein that anchors the thick filament to the Z-disk[29].

Cardiac Electrophysiology

This section will briefly explain how action potentials (APs) occur in myocytes, propagate to surrounding tissue, and signal the tissue to contract. Therefore, this introduction to cardiac electrophysiology begins with the individual myocyte, followed by increasing detail regarding interacting structures, which make AP propagation through the tissue possible.

Cellular Electrophysiology

Passive Electrical Properties

As explained earlier, the sarcolemma prevents charged molecules from entering or exiting the cell without a protein in the membrane to allow such transport. Commonly, cells hold and maintain ion concentration gradients, which also establishes electrical gradients across the membrane due to the charge of ions. Na^+ and K^+ are the most important ions in establishing this electrochemical gradient. The cell maintains the gradient via the Na^+-K^+ pump, which pumps Na^+ out of the cell while pumping K^+ into the cell[30]. Calcium also contributes to the electrical gradient, but plays a larger role in excitation contraction coupling, which will be discussed in detail later.

These gradients establish electrical voltages for each ion type separated by the cell membrane and each voltage can be described by the Nernst equation:

$$E_I = \frac{RT}{z_I F} \ln \frac{[I]_o}{[I]_i}$$

with the voltage for a specific ion E_I, the gas constant R, the temperature in Kelvin T, the valence of the specific ion z_I, Faraday's constant F, the ion concentration inside the cell $[I]_i$ and the ion concentration outside the cell $[I]_o$. The voltage described by the Nernst equation is also called ion equilibrium voltage. This is due to the voltage measured when electrical and chemical gradients come to equilibrium for a specific ion. As an example, the equilibrium voltage for Na^+ is +70 mV when the respective extra/intracellular Na^+ concentrations are 125 and 7.5 mM, at 295° Kelvin.

Since the membrane is permeable to K^+, Na^+, and chlorine (Cl^-) a more comprehensive description of the voltage at rest is the Goldman-Hodgkin-Katz equation:

$$E = \frac{RT}{F} \ln \frac{P_{Na}[Na]_o + P_K[K]_o + P_{Cl}[Cl]_i}{P_{Na}[Na]_i + P_K[K]_i + P_{Cl}[Cl]_o}$$

with the permeability P of the respective ions as noted by subscript. In other words, the flow of ions across the membrane generates a membrane voltage dependent on the electrochemical concentration gradient of the ions as well as the permeability state of the respective ion channels. If you assume that Cl^- permeability is very low, the Cl terms can be ignored. When a myocyte is at rest the permeability of K^+ is roughly one hundred times larger than the permeability of Na^+. Due to the high K^+ concentration inside in

contrast to outside of the cell the resting voltage of the mammalian myocyte is around -80 mV[30, 31].

The membrane permeability for a specific ion can be modeled as a resistance, and the equilibrium voltage for the same ion can be modeled as a voltage source. Using these models, an electrical schematic is commonly applied to describe a segment of the membrane (Fig. 1.4). The composite permeability of the sarcolemma to the various ions, as described in the Goldman-Hodgkin-Katz equation, determines the membrane resistance[12].

In order to have a capacitor, two conductors (the extracellular fluid and intracellular fluid) need to be separated by an insulator (the cell membrane). Capacitance is influenced by the thickness, surface area, and electrical dielectric of the insulator. Mathematically the capacitance C is described by:

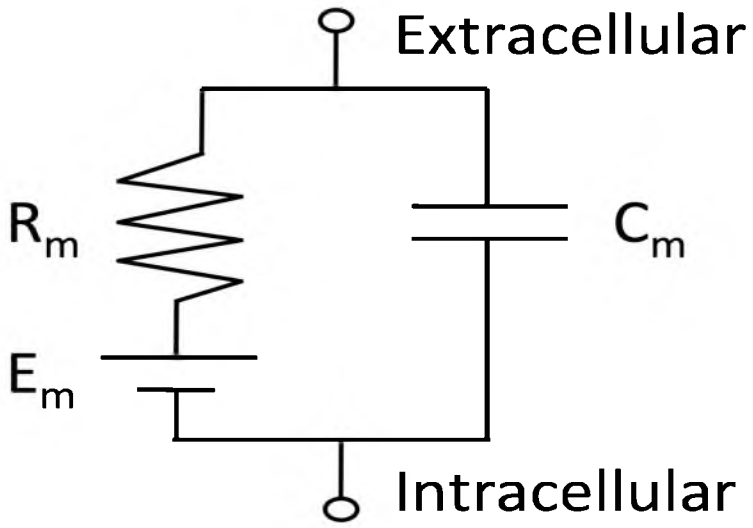

Figure 1.4: Schematic representing the circuit equivalent of a small sarcolemmal segment at rest. It shows a composite membrane resistance of the permeable ions, R_m, and the membrane capacitance, C_m. The membrane voltage, E_m, is dependent on ion concentration and permeability of all permeable ions. An extended version of this schematic, showing variable resistances and reversal voltages for certain ions, is found in Hodgkin and Huxley's work[5].

$$C = \frac{\varepsilon \varepsilon_0 A}{d}$$

with the dielectric constant of the insulator ε, the dielectric constant of vacuum ε_0, the surface area A, and the thickness of the insulator d. Cells exhibit significant variability of their membrane area, but the relative dielectric constant ε and the thickness d of their membrane is typically viewed as constant. In previous studies it has been speculated that the surface area of a myocyte may change with strain or contraction, leading to a change in capacitance[32, 33]. Another study reported membrane capacitance that was insensitive to strain, but the membrane area of the cell affected was small compared to the rest of the cell[34].

Membrane Excitability

Many ion channels in the myocyte are voltage sensitive, with increased opening probabilities when the membrane voltage reaches specific thresholds. For example, the inward rectifying K^+ channel has high open probabilities when the membrane voltage is close to the resting voltage. The sodium channel, on the other hand, opens when the membrane depolarizes to a threshold voltage and remains in an open state for a short period of time before inactivating[35]. For a more extensive description on ion channel function the interested reader is referred to pertinent textbooks, for example, *Ion channels of excitable membranes*, chapter 2[12].

An important property of sodium channels is their fast inactivation, which is maintained until the membrane is repolarized. This is important for activation of an AP. When a part of the sarcolemma depolarizes and the threshold voltage is reached, Na^+ will flow through the channel further depolarizing the adjacent membrane and activating the

Na^+ channels there. The newly activated channels will open, speeding depolarization of the membrane in a positive feedback loop[9, 31], which forms a local circuit. This form of activation can happen only if the Na^+ channels are available for activation, not inactivated. The more inactivated Na^+ channels present the slower activation propagates until the myocyte and the tissue is inexcitable[36].

Stretch Modulated Ion Channels

Many types of ion channels alter their properties in response to deformation of the cell membrane. These channels are called mechanosensitive. An example for a mechanosensitive ion channel is the inward rectifying K^+ channel, which has been shown to exhibit reduced currents when strain is applied[34, 37]. Ion channels specialized in sensing of mechanical alterations are stretch-activated and swelling-activated channels. These channels respond to the deformation by either opening or closing. An example is the stretch-activated transient receptor potential cation (TRPC6) channels, which is thought to conduct stretch-activated nonspecific ion currents in cardiac myocytes.

A number of models have been developed to describe currents through stretch-activated ion channels. An example from an early model assumed a reverse potential E_{Ns} of -30 mV, a maximum conductance G_{Ns} of 1 μS and an exponential effect of stain on the current:

$$I_{Ns} = G_{Ns} \frac{1}{1 + e^{-5(SL-2)}} \left(V_m - E_{Ns}\right)$$

with the sarcomere length SL and the membrane voltage V_m[38].

Gap Junction Channels

Gap junctions play a critical role in local circuit activation propagating from one myocyte to the adjacent. It is through gap junction channels that cardiac cells are electrically coupled together. If the gap junction channel conductance is too high, the cells will be highly coupled increasing electrical load on a myocyte, which will prevent sufficient charge accumulation needed for the voltage to reach the threshold of activation[39]. As the myocytes become less coupled the intercellular resistance increases promoting a decrease in conduction velocity until becoming effectively decoupled, leading to conduction block[36]. For those interested in more detail regarding the influence of gap junctions on conduction velocity see[39, 40].

Tissue Electrophysiology

Initial concepts of cardiac tissue electrophysiology have been derived from descriptions of electrical properties and conduction in neurons[5]. In both fields, an established model to describe propagation of electrical signals is the cable model:

$$\frac{1}{R_i}\frac{\partial^2 V_m}{\partial x^2} = C_m\frac{\partial V_m}{\partial t} + \frac{V_m}{R_m}$$

with the membrane resistance per area R_m, intracellular resistance R_i, membrane capacitance per area C_m, and membrane voltage V_m. The intracellular current (left hand side) equals the capacitive and resistive currents (right hand side) due to the membrane capacitance and resistance, respectively. As described earlier, there is some controversy regarding the effects of strain on membrane capacitance. Due to the strong effect membrane capacitance has on conduction velocity[41], it would be important to know if

strain does affect membrane capacitance. Similarly, it would be important to know if and how strain affects the intracellular and membrane resistances.

More commonly in cardiac modeling, two- and three-dimensional mono- and bidomain approaches are used to describe propagation of electrical activation in cardiac tissue. These approaches need knowledge about cellular electrophysiology and electrical properties of the tissue. The bidomain model allows for calculating the currents through the intracellular and extracellular spaces as well as voltage generated by current crossing the cell membrane. A drawback to using the bidomain model is that it is computationally expensive, in particular, for large volumes. This calculation is done using intracellular and extracellular conductivities, which are dependent on the respective volumes. The monodomain is an alternative that is based on lumping intracellular and extracellular conductivities by a bulk conductivity tensor. The defining equation of the monodomain is:

$$\frac{\partial V_m}{\partial t} = \frac{1}{\beta C_m}\left\{\nabla\cdot\left(G\nabla V_m\right) - \beta\left(I_{ion} + I_s\right)\right\}$$

with the surface to volume ratio β, bulk conductivity tensor G, the currents through the cell membrane I_{ion}, and the stimulus current I_s. Using the monodomain description can be an appropriate approximation when modeling AP propagation because there is little difference to bidomain simulations[42], given there are no current sources within the extracellular space to model defibrillation, for example[43].

Excitation Contraction Coupling

Electrical activation of myocytes causes cellular contraction. For this to happen the electrical signal needs to be transduced to mechanical contractions. During this process of

excitation contraction coupling APs are transduced to a calcium signal, which in turn triggers and modulates mechanical contraction. This topic has been extensively researched[44-48].

Depolarization of the membrane activates voltage sensitive calcium channels (Fig. 1.5), which open allowing calcium into the junctional space between the sarcolemma and the sarcoplasmic reticulum (SR). The increase in Ca^{2+} concentration in the junctional space leads to Ca^{2+} binding to ryanodine receptors (RyR) in SR membrane, causing the RyR to open releasing Ca^{2+} from the SR into the junctional space. The transient increase in calcium quickly decays after closure and inactivation of the calcium channels and RyRs, respectively. The sarcoplasmic reticulum calcium ATP-ase (SERCA) pump

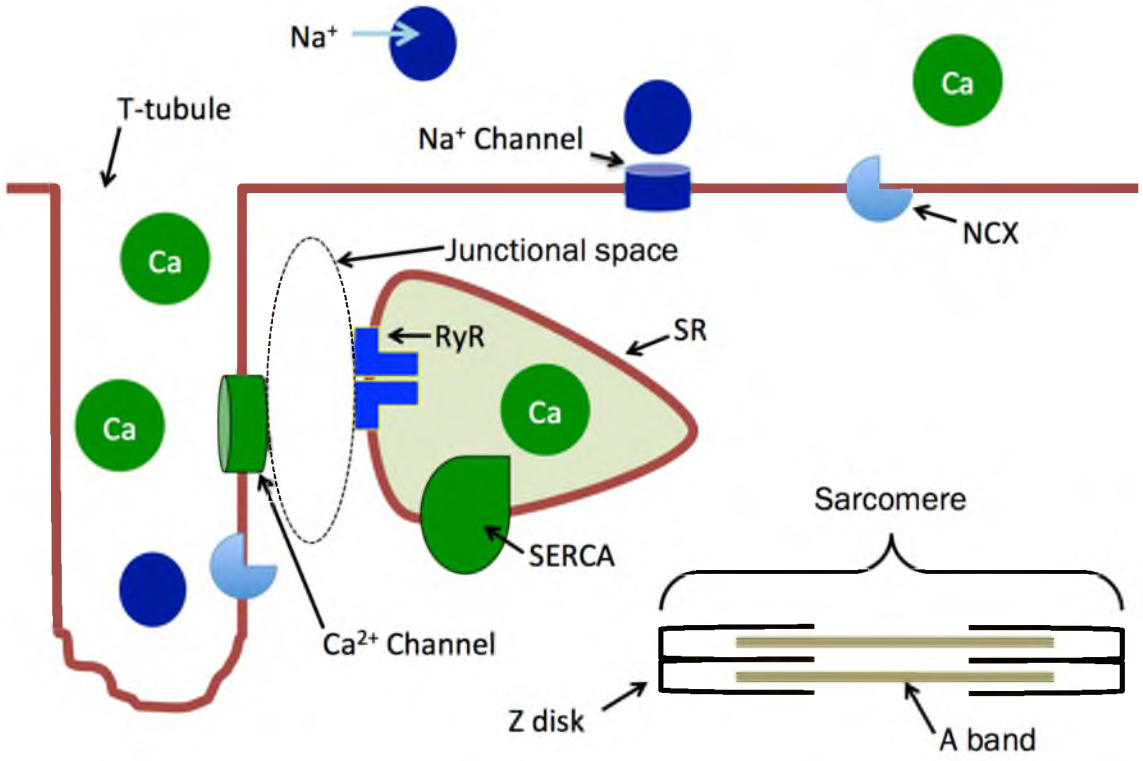

Figure 1.5: Diagram representing the important proteins and ions involved in excitation contraction coupling. Na^{+}: Sodium ions; Ca: Calcium ions; RyR: Ryanodine receptors; SR: Sarcoplasmic reticulum; SERCA: Sarcoplasmic calcium ATPase (pump).

returns calcium to the SR, and the Na^{+}-Ca^{2+} exchanger together with a sarcolemmal Ca pump transport calcium to the extracellular space.

As described earlier, troponin and tropomyosin cover the actin at rest preventing the myosin heads from attaching and contracting[49]. As the cytosolic Ca^{2+} concentration increases troponin binds to Ca^{2+} causing the tropomyosin to move; this reveals the binding site for myosin and induces contraction. Through a major part of systole the Na^{+}-Ca^{2+} exchanger moves Ca^{2+} into the extracellular space while moving Na^{+} into the intracellular space. The removal of Ca^{2+} by way of the SERCA pump and the Na^{+}-Ca^{2+} exchanger leads to Ca^{2+} unbinding from troponin, tropomyosin covering the binding region of actin, and myocytes relaxing[49].

It is interesting to note that the process of force development at whole heart but also cellular level has been reported to change due to mechanical deformation. The Frank-Starling law, for example, explains an immediate change in the force of contraction depending on the preload[50]. Further studies showed that, when strain is continuously applied for a number of minutes the force of contraction, along with the calcium transient amplitude, increases[51]. Another study suggested that the sarcoplasmic reticulum leaks more calcium into the cytosolic space when strain is applied, but the experiment showed a decrease from strained spark rate to control levels over the course of a minute[52].

Strain and Heart Disease

Heart disease has been the lead cause of death among Americans for many years. In 2006 over 600,000 people died of heart disease, which is above 25% of all deaths that year[53]. A study examining the mechanisms of cardiac arrest in those suffering from heart failure found that only 10% of those who died were because of electromechanical

dissociation[54]. Thus, it may be implied that the majority of those who die of heart disease suffer from some form of electrical arrhythmia. It is has been speculated that strain is involved in arrhythmogenesis[55]. Furthermore, it is thought that strain induces changes in expression of proteins involved in electrical signaling[56].

Arrhythmias

It has been hypothesized that remodeling of protein expressions in atrial fibrillation (AF) is caused by changes of strain and that this remodeling leads to further remodeling of electrical activity[57]. Some mechanisms that induce AF include mitral valve regurgitation, mitral stenosis, and heart failure[58]. When the mitral valve remains open or closes incompletely during ventricular contraction, pressure in the left atrium is increased. An increase in pressure in the left atrium also occurs when a valve is affected by stenosis, but the increased pressure is due to the incomplete opening of the valve. Though it is clear that mechanical stimulation plays a role in the development and progression of AF[59, 60], the mechanisms involved in signaling protein remodeling are not clearly understood.

Commotio cordis occurs when cardiac arrest follows a blunt trauma to the heart[61]. There may be few who die due to this induced ventricular arrhythmia, but it is evidence that mechanical deformation of the heart will cause immediate electrical changes[55, 62]. The effect of mechanical impacts on the heart has been modeled by activating stretch activated ion channels[62], but may also be due to conduction block at large strain[63], the mechanism of which remains unexplained.

Heart Failure

Heart failure, like AF, also has a close connection to mechanical stimuli. One of the animal models used to induce heart failure involves surgically inducing aortic stenosis[64-66], which increases the mechanical load on the left ventricle. Another way heart failure can develop naturally occurs after a portion of the heart has become infarct[67, 68]. The dead tissue no longer contracts, increasing the mechanical demand on the remaining portion of the heart that is still functional. It is interesting to note that patients suffering with aortic stenosis, hypertension, dilated cardiomyopathy, and cardiac failure show increased sensitivity towards arrhythmias[69, 70]. This suggests that the pathophysiological contraction of the heart affects the electrical activity of the heart[71].

It is well-known that people who have an increased cardiac demand through exercise or pregnancy also have cardiac hypertrophy[67]. A study looking at the effects of exercise showed that hypertrophied hearts from rats placed on a rigorous exercise schedule had a similar t-tubule density to that of normal rat hearts[8]. Hypertrophied hearts that developed due to aortic stenosis however showed a decreased t-tubule density compared to normal hearts[8]. While it is clear that mechanical stimuli can lead to remodeling of the heart, it remains unclear how the physiological stimuli differ from the pathophysiological stimuli.

References

1. Silverthorn DU. *Human physiology: An integrated approach*. Upper Saddle River, New Jersey: Prentice Hall; 2001.

2. Randall DJ, Burggren W, French K. *Ekert animal physiology : Mechanisms and adaptations*. New York: W. H. Freeman and Company; 2002.

3. Berne RM, Levy MN, Koeppen BM, Stanton BA. *Physiology*. St. Louis: Mosby; 1998.

4. Alberts B, Johnson A, Lewis J, Raff M, Roberts K, Walter P. *Molecular biology of the cell*. New York, New York: Garland Science; 2002.

5. Hodgkin AL, Huxley AF. A quantitative description of membrane current and its application to conduction and excitation in nerve. *J Physiol*. 1952;117:500-544

6. Lackey DP, Carruth ED, Lasher RA, Boenisch J, Sachse FB, Hitchcock RW. Three-dimensional modeling and quantitative analysis of gap junction distributions in cardiac tissue. *Ann Biomed Eng*. 2011;39:2683-2694

7. Campbell SE, Gerdes AM, Smith TD. Comparison of regional differences in cardiac myocyte dimensions in rats, hamsters, and guinea pigs. *Anat Rec*. 1987;219:53-59

8. Kemi OJ, Hoydal MA, Macquaide N, Haram PM, Koch LG, Britton SL, Ellingsen O, Smith GL, Wisloff U. The effect of exercise training on transverse tubules in normal, remodeled, and reverse remodeled hearts. *J Cell Physiol*. 2010

9. Fozzard HA. Conduction of the action potential. In: Berne RM, Sperelakis N, Geiger SR, eds. *Handbook of physiology*. Washington, DC: American Physiological Society; 1979:335-356.

10. Preston G, Carroll T, Guggino W, Agre P. Appearance of water channels in xenopus oocytes expressing red cell chip28 protein. *Science*. 1992;256:385-387

11. Bridge JH, Smolley JR, Spitzer KW. The relationship between charge movements associated with ica and ina-ca in cardiac myocytes. *Science*. 1990;248:376-378

12. Hille B. *Ion channels of excitable membranes*. Sunderland, Mass.: Sinauer; 2001.

13. Desplantez T, Dupont E, Severs NJ, Weingart R. Gap junction channels and cardiac impulse propagation. *J Membr Biol*. 2007;218:13-28

14. Simon AM, Goodenough DA. Diverse functions of vertebrate gap junctions. *Trends Cell Biol*. 1998;8:477-483

15. Goldberg GS, Lampe PD, Nicholson BJ. Selective transfer of endogenous metabolites through gap junctions composed of different connexins. *Nat Cell Biol*. 1999;1:457-459

16. Pásek M, Brette F, Nelson A, Pearce C, Qaiser A, Christe G, Orchard C. Quantification of t-tubule area and protein distribution in rat cardiac ventricular myocytes. *Prog Biophys Mol Biol*. 2008:244-257

17. Brette F, Orchard C. T-tubule function in mammalian cardiac myocytes. *Circ Res*. 2003;92:1182-1192

18. Brette F, Sallé L, Orchard C. Quantification of calcium entry at the t-tubules and surface membrane in rat ventricular myocytes. *Biophys J.* 2006;90:381-389

19. Louch WE, Sejersted OM, Swift F. There goes the neighborhood: Pathological alterations in t-tubule morphology and consequences for cardiomyocyte Ca2+ handling. *J Biomed Biotechnol.* 2010;2010:503906

20. Tidball JG, Cederdahl JE, Bers DM. Quantitative analysis of regional variability in the distribution of transverse tubules in rabbit myocardium. *Cell Tissue Res.* 1991;264:293-298

21. Fawcett DW, McNutt NS. The ultrastructure of the cat myocardium. I. Ventricular papillary muscle. *J Cell Biol.* 1969;42:1-45

22. Soeller C, Cannell MB. Examination of the transverse tubular system in living cardiac rat myocytes by 2-photon microscopy and digital image-processing techniques. *Circ Res.* 1999;84:266-275

23. Savio-Galimberti E, Frank J, Inoue M, Goldhaber JI, Cannell MB, Bridge JH, Sachse FB. Novel features of the rabbit transverse tubular system revealed by quantitative analysis of three-dimensional reconstructions from confocal images. *Biophys J.* 2008;95:2053-2062

24. Kaprielian RR, Stevenson S, Rothery SM, Cullen MJ, Severs NJ. Distinct patterns of dystrophin organization in myocyte sarcolemma and transverse tubules of normal and diseased human myocardium. *Circulation.* 2000;101:2586-2594

25. Kostin S, Scholz D, Shimada T, Maeno Y, Mollnau H, Hein S, Schaper J. The internal and external protein scaffold of the t-tubular system in cardiomyocytes. *Cell Tissue Res.* 1998;294:449-460

26. Zeng T, Bett GC, Sachs F. Stretch-activated whole cell currents in adult rat cardiac myocytes. *Am J Physiol Heart Circ Physiol.* 2000;278:H548-557

27. Sachs F. Stretched activated channels in the heart. In: Kohl P, Sachs F, Franz MR, eds. *Cardiac mechano-electric feedback and arrythmias from pipette to patient.* Philadelphia, PA: Elsevier Saunders; 2005:2-9.

28. Gordon AM, Homsher E, Regnier M. Regulation of contraction in striated muscle. *Physiol Rev.* 2000;80:853-924

29. Granzier HL, Irving TC. Passive tension in cardiac muscle: Contribution of collagen, titin, microtubules, and intermediate filaments. *Biophys J.* 1995;68:1027-1044

30. Berne RM, Sperelakis N, American Physiological Society (1887-). *The cardiovascular system.* Bethesda, Md. Baltimore, Md.: American Physiological Society ; distributed by Williams and Wilkins Co.; 1979.

31. Woodbury JW. Action potential: Properties of excitable membranes. In: Ruch TC, Patton HD, eds. *Physiology and biophysics*. Philadephia: W. B. Saunders Company; 1966:26-68.

32. Kohl P, Cooper PJ, Holloway H. Effects of acute ventricular volume manipulation on in situ cardiomyocyte cell membrane configuration. *Prog Biophys Mol Biol.* 2003;82:221-227

33. Mills RW, Narayan SM, McCulloch AD. Mechanisms of conduction slowing during myocardial stretch by ventricular volume loading in the rabbit. *Am J Physiol Heart Circ Physiol.* 2008;295:H1270-H1278

34. Isenberg G, Kazanski V, Kondratev D, Gallitelli MF, Kiseleva I, Kamkin A. Differential effects of stretch and compression on membrane currents and [Na+]c in ventricular myocytes. *Prog Biophys Mol Biol.* 2003;82:43-56

35. Opie LH. *The heart physiology, from cell to circulation.* Philadelphia, PA: Lippincott-Raven; 1998.

36. Shaw RM, Rudy Y. Ionic mechanisms of propagation in cardiac tissue. Roles of the sodium and l-type calcium currents during reduced excitability and decreased gap junction coupling. *Circ Res.* 1997;81:727-741

37. Dyachenko V, Husse B, Rueckschloss U, Isenberg G. Mechanical deformation of ventricular myocytes modulates both TRPC6 and Kir2.3 channels. *Cell Calcium.* 2009;45:38-54

38. Noble D, Varghese A, Kohl P, Noble P. Improved guinea-pig ventricular cell model incorporating a diadic space, Ikr and Iks, and length- and tension-dependent processes. *Can J Cardiol.* 1998;14:123-134

39. Cascio WE, Yang H, Muller-Borer BJ, Johnson TA. Ischemia-induced arrhythmia: The role of connexins, gap junctions, and attendant changes in impulse propagation. *J Electrocardiol.* 2005;38:55-59

40. Rohr S. Role of gap junctions in the propagation of the cardiac action potential. *Cardiovasc Res.* 2004;62:309-322

41. McNary TG, Sohn K, Taccardi B, Sachse FB. Experimental and computational studies of strain-conduction velocity relationships in cardiac tissue. *Prog Biophys Mol Biol.* 2008;97:383-400

42. Potse M, Dube B, Richer J, Vinet A, Gulrajani RM. A comparison of monodomain and bidomain reaction-diffusion models for action potential propagation in the human heart. *IEEE Trans Biomed Eng.* 2006;53:2425-2435

43. Clayton RH, Bernus O, Cherry EM, Dierckx H, Fenton FH, Mirabella L, Panfilov AV, Sachse FB, Seemann G, Zhang H. Models of cardiac tissue

electrophysiology: Progress, challenges and open questions. *Prog Biophys Mol Biol*. 2011;104:22-48

44. Fabiato A, Fabiato F. Calcium and cardiac excitation-contraction coupling. *Annu Rev Physiol*. 1979;41:473-484

45. Bers DM. Cardiac excitation-contraction coupling. *Nature*. 2002;415:198-205

46. Ozawa T. Modulation of ryanodine receptor Ca2+ channels (review). *Mol Med Report*. 2010;3:199-204

47. Huxley HE. The mechanism of muscular contraction. *Science*. 1969;164:1356-1365

48. Williams GS, Smith GD, Sobie EA, Jafri MS. Models of cardiac excitation-contraction coupling in ventricular myocytes. *Math Biosci*. 2010;226:1-15

49. Schaub MC, Perry SV. The relaxing protein system of striated muscle. Resolution of the troponin complex into inhibitory and calcium ion-sensitizing factors and their relationship to tropomyosin. *Biochem J*. 1969;115:993-1004

50. Gordon AM, Huxley AF, Julian FJ. The variation in isometric tension with sarcomere length in vertebrate muscle fibres. *J Physiol*. 1966;184:170-192

51. Allen DG, Kurihara S. The effects of muscle length on intracellular calcium transients in mammalian cardiac muscle. *J Physiol*. 1982;327:79-94

52. Iribe G, Ward CW, Camelliti P, Bollensdorff C, Mason F, Burton RA, Garny A, Morphew MK, Hoenger A, Lederer WJ, Kohl P. Axial stretch of rat single ventricular cardiomyocytes causes an acute and transient increase in Ca2+ spark rate. *Circ Res*. 2009;104:787-795

53. Heron M, Hoyert DL, Murphy SL, Xu J, Kochanek KD, Tejada-Vera B. Deaths: Final data for 2006. *Natl Vital Stat Rep*. 2009;57:1-134

54. Luu M, Stevenson WG, Stevenson LW, Baron K, Walden J. Diverse mechanisms of unexpected cardiac arrest in advanced heart failure. *Circulation*. 1989;80:1675-1680

55. Link MS, Maron BJ, Estes NAM. Ventricular fibrillation secondary to nonpenetrating chest wall impact (commotio cordis). In: Kohl P, Franz MR, Sachs F, eds. *Cardiac mechano-electric feedback and arrhythmias*. Philadelphia, PA: Elsevier Saunders; 2005:137-144.

56. Suzuki T, Yamazaki T. Stretch effects on second messengers and early gene expression. In: Kohl P, Franz MR, Sachs F, eds. *Cardiac mechano-electric feedback and arrhythmias*. Philadelphia, PA: Elsevier Saunders; 2005:63-69.

57. Wijffels MC, Kirchhof CJ, Dorland R, Allessie MA. Atrial fibrillation begets atrial fibrillation. A study in awake chronically instrumented goats. *Circulation*. 1995;92:1954-1968

58. Kalman JM, Sanders P, Morton JB. Mechanically induced electrical remodeling in human atrium. In: Kohl P, Franz MR, Sachs F, eds. *Cardiac mechano-electric feedback and arrhythmias*. Philadelphia, PA: Elsevier Saunders; 2005:220-228.

59. Camm AJ, Yusuf S. Atrial fibrillation and dilated cardiomyopathy. In: Kohl P, Franz MR, Sachs F, eds. *Cardiac mechano-electric feedback and arrhythmias*. Philadelphia, PA: Elsevier Saunders; 2005:229-239.

60. Schotten U, Allessie M. The substrate of atrial fibrillation in chronically dilated atria. In: Kohl P, Franz MR, Sachs F, eds. *Cardiac mechano-electric feedback and arrhythmias*. Philadelphia, PA: Elsevier Saunders; 2005:154-163.

61. Link MS, Estes NAM, Maron BJ. Sudden death caused by chest wall trauma (commotio cordis). In: Kohl P, Franz MR, Sachs F, eds. *Cardiac mechano-electric feedback and arrhythmias*. Philadelphia, PA: Elsevier Saunders; 2005:270-276.

62. Garny A, Kohl P. Mechanical induction of arrhythmias during ventricular repolarization: Modeling cellular mechanisms and their interaction in two dimensions. *Ann N Y Acad Sci*. 2004;1015:133-143

63. Eijsbouts SC, Majidi M, van Zandvoort M, Allessie MA. Effects of acute atrial dilation on heterogeneity in conduction in the isolated rabbit heart. *J Cardiovasc Electrophysiol*. 2003;14:269-278

64. Rannou F, Sainte-Beuve C, Oliviero P, Do E, Trouve P, Charlemagne D. The effects of compensated cardiac hypertrophy on dihydropyridine and ryanodine receptors in rat, ferret and guinea-pig hearts. *J Mol Cell Cardiol*. 1995;27:1225-1234

65. Milnes JT, MacLeod KT. Reduced ryanodine receptor to dihydropyridine receptor ratio may underlie slowed contraction in a rabbit model of left ventricular cardiac hypertrophy. *J Mol Cell Cardiol*. 2001;33:473-485

66. Wang X, Gerdes AM. Chronic pressure overload cardiac hypertrophy and failure in guinea pigs: Iii. Intercalated disc remodeling. *J Mol Cell Cardiol*. 1999;31:333-343

67. Hill JA, Olson EN. Cardiac plasticity. *N Engl J Med*. 2008;358:1370-1380

68. Gomez AM, Guatimosim S, Dilly KW, Vassort G, Lederer WJ. Heart failure after myocardial infarction: Altered excitation-contraction coupling. *Circulation*. 2001;104:688-693

69. Taggart P. Mechano-electric feedback in the human heart. *Cardiovasc Res*. 1996;32:38-43

70. Taggart P, Sutton PM. Cardiac mechano-electric feedback in man: Clinical relevance. *Prog Biophys Mol Biol*. 1999;71:139-154

71. Kohl P, Hunter P, Noble D. Stretch-induced changes in heart rate and rhythm: Clinical observations, experiments and mathematical models. *Prog Biophys Mol Biol*. 1999;71:91-138

2. EXPERIMENTAL AND COMPUTATIONAL STUDIES OF STRAIN–CONDUCTION VELOCITY RELATIONSHIPS IN CARDIAC TISSUE

Reprinted with permission from Progress in Biophysics and Molecular Biology 97 (2008) 383-400

Available online at www.sciencedirect.com
ScienceDirect
Progress in Biophysics and Molecular Biology 97 (2008) 383–400
Progress in Biophysics & Molecular Biology
www.elsevier.com/locate/pbiomolbio

Experimental and computational studies of strain–conduction velocity relationships in cardiac tissue

T.G. McNary[a,b], K. Sohn[a,b], B. Taccardi[a,c], F.B. Sachse[a,b,*]

[a]*Nora Eccles Harrison Cardiovascular Research and Training Institute, University of Utah, 95 S 2000 E, Salt Lake City, UT 84112, USA*
[b]*Bioengineering Department, University of Utah, 72 S Central Campus Drive, Salt Lake City, UT 84112, USA*
[c]*School of Medicine, University of Utah, 30 N 1900 E, Salt Lake City, UT 84132, USA*

Available online 29 February 2008

Abstract

Velocity of electrical conduction in cardiac tissue is a function of mechanical strain. Although strain-modulated velocity is a well established finding in experimental cardiology, its underlying mechanisms are not well understood. In this work, we summarized potential factors contributing to strain–velocity relationships and reviewed related experimental and computational studies. We presented results from our experimental studies on rabbit papillary muscle, which supported a biphasic relationship of strain and velocity under uni-axial straining conditions. In the low strain range, the strain–velocity relationship was positive. Conduction velocity peaked with 0.59 m/s at 100% strain corresponding to maximal force development. In the high strain range, the relationship was negative. Conduction was reversibly blocked at $118 \pm 1.8\%$ strain. Reversible block occurred also in the presence of streptomycin. Furthermore, our studies revealed a moderate hysteresis of conduction velocity, which was reduced by streptomycin. We reconstructed several features of the strain–velocity relationship in a computational study with a myocyte strand. The modeling included strain-modulation of intracellular conductivity and stretch-activated cation non-selective ion channels. The computational study supported our hypotheses, that the positive strain–velocity relationship at low strain is caused by strain-modulation of intracellular conductivity and the negative relationship at high strain results from activity of stretch-activated channels. Conduction block was not reconstructed in our computational studies. We concluded this work by sketching a hypothesis for strain-modulation of conduction and conduction block in papillary muscle. We suggest that this hypothesis can also explain uni-axially measured strain–conduction velocity relationships in other types of cardiac tissue, but apparently necessitates adjustments to reconstruct pressure or volume related changes of velocity in atria and ventricles.
Published by Elsevier Ltd.

Keywords: Strain–conduction velocity relationship; Mechano-electric feedback; Cardiac electrophysiology; Strain-modulated ion channels; Strain-modulated tissue conductivity

*Corresponding author at: Nora Eccles Harrison Cardiovascular Research and Training Institute, University of Utah, 95 S 2000 E, Salt Lake City, UT 84112, USA. Tel.: +1 801 587 9514; fax: +1 801 581 3128.
E-mail addresses: mcnary@cvrti.utah.edu (T.G. McNary), sohn@cvrti.utah.edu (K. Sohn), taccardi@cvrti.utah.edu (B. Taccardi), fs@cvrti.utah.edu (F.B. Sachse).

0079-6107/$ - see front matter Published by Elsevier Ltd.
doi:10.1016/j.pbiomolbio.2008.02.023

Contents

1. Introduction

The relationship between mechanical strain and velocity of electrical conduction in cardiac tissues has been studied since the 1960s. Experimental studies have been carried out with different species and types of cardiac tissue (Penefsky and Hoffman, 1963; Spear and Moore, 1972; Dominguez and Fozzard, 1979; Rosen et al., 1981; Tavi et al., 1996; Zhu et al., 1997; Eijsbouts et al., 2003; Sung et al., 2003; Sachse et al., 2004). These studies showed differing effects of strain on conduction velocity. More recently, these studies were complemented by computational studies based on mathematical models of cellular and tissue electrophysiology (Rice et al., 1998; Sachse et al., 2000, 2002, 2006, 2007; Trayanova et al., 2004; Kuijpers et al., 2007). Those studies also showed differing results for various species and tissue types. The heterogeneity of experimental and computational findings, the biophysical mechanisms underlying strain–velocity relationships, and the physiological relevance of this mechano-electric feedback phenomenon are still not completely understood.

In this work, we describe factors at cellular and tissue level contributing to the strain–velocity relationship in cardiac tissue, followed by a review of experimental and computational studies of these relationships. In the review we provide quantitative data on strain–velocity relationships for various species and experimental conditions. Furthermore, we classified the experimental and computational data into different types of strain–velocity relationships: biphasic, constant, increasing and decreasing.

We present then the design and results of our experimental study on rabbit papillary muscle. Conduction in rabbit papillary muscle has been well characterized in various studies in the past and the preparation allows for reliable measurement of one-dimensional mechanical strain.[1] Our study was conducted to gain insights in biophysical mechanisms of the strain–velocity relationship in ventricular tissue and developing a qualitative description of this relationship.

Our study showed novel phenomena of strain–velocity relationships, in particular reversible block of conduction for large strain and hysteresis of conduction velocity in a protocol with increasing and decreasing

[1] We refer to Appendix A for a description of strain measures used in this work.

strain. We explored hypotheses for biophysical mechanisms underlying the measured strain–velocity relationships in computational studies with a one-dimensional model of electrical conduction in cardiac tissue. In particular, we were interested in discriminating the effects of strain-modulated electrical conductivity of myocardium and activity of mechano-sensitive ion channels on conduction velocity.

We conclude with discussing our findings, relating these to results of others, and proposing a hypothesis for conduction in uni-axially strained cardiac tissue. The hypothesis was developed by comparison of our experimental and computational findings and groups the effect on conduction velocity according to the level of strain.

2. Background

2.1. Factors contributing to strain–velocity relationships

Cardiac conduction velocity is a function of cellular electrophysiology and electrical properties of tissue. In the following, we will list factors contributing to the strain-dependent modulation of cellular and tissue properties, which were suggested to affect strain–conduction velocity relationships.

At the cellular level, strain and tension of the sarcolemma were found to activate and modulate current flow through various ion channels. Strain depolarized the resting transmembrane voltage V_{rest} of cardiomyocytes (Deck, 1964; Rosen et al., 1981), changed the shape of action potentials (Deck, 1964; Spear and Moore, 1972; Zabel et al., 1996a; Riemer and Tung, 2003) and reduced action potential duration (APD) (White et al., 1993; Hsieh et al., 1999).

These changes were commonly explained by increased open state probabilities of mechano-sensitive channels, in particular the stretch-activated cation non-selective channels (nsSACs) (Zhang et al., 2000). Blocking of nsSACs is possible with gadolinium, streptomycin and GsMTx-4 (Franz and Bode, 2003; Calaghan and White, 2004; Sachs, 2004; White, 2006). Recently, the protein forming these channels in cells of vertebrates was identified as the canonical transient receptor potential channel (TRPC1) (Maroto et al., 2005). The increased V_{rest} due to opening of nsSACs was suggested to underly slowing of conduction velocity by voltage-dependent inactivation of fast sodium channels (Rice et al., 1998; Mills et al., 2005; Sachse et al., 2006). These sodium channels are responsible for the upstroke of myocytes' action potential and upstroke velocity is known to be related to conduction velocity.

Further channels with reported strain-modulation include those associated with inward rectifier potassium, sarcolemmal ATP-sensitive potassium and outward rectifier potassium currents (Ruknudin et al., 1993; Niu and Sachs, 2003; Li et al., 2006). The physiological role of the strain-modulation of these potassium channels and their significance in strain–conduction velocity relationships is unclear. A proposed role of the outward rectifier potassium current through two-pore domain channels TREK-1 was to counterbalance nsSAC currents when myocytes are stretched at end diastole (Li et al., 2006). This effect would reduce membrane depolarization by opening of nsSACs and sodium channel inactivation.

It was also suggested that strain uncovers "surplus" sarcolemma and expands sarcolemmal vesicles (Kohl et al., 2003; Calaghan, 2007). These changes would affect membrane capacitance and accessibility of transmembrane proteins. An increase of membrane capacitance would reduce conduction velocity by slowing depolarization.

Further effects of strain on electrical properties were proposed at tissue level and characterized in computational studies of ventricular myocardium (Sachse et al., 2000). Here, strain-modulation of intracellular electrical conductivity was found to have varied effects on conduction velocity. A positive relationship of strain and intracellular conductivity led to positive strain–conduction velocity relationships. Strain-independent conductivity led to negative strain–conduction velocity relationships (see Section 2.3).

2.2. Review of experimental studies

An overview of experimental studies on conduction velocity is given in Table 1. We classified the experimental results in the following listing into four groups: biphasic, constant, increasing and decreasing relationships of strain versus conduction velocity.

Table 1
Experimental studies of the strain–conduction velocity relationship in cardiac tissue

Year	Authors and reference	Species	Tissue	Dim.	Relationship
1963	Penefsky and Hoffman (1963)	Cat	Papillary muscle	1	Biphasic
		Cat	Auricle strip	1	Biphasic
		Hamster	Ventricular strip	1	Biphasic
		Squirrel	Ventricular strip	1	Biphasic
		Chicken	Auricle strip	1	Biphasic
		Chicken	Ventricular strip	1	Biphasic
		Terrapin	Auricle strip	1	Biphasic
		Terrapin	Ventricular strip	1	Biphasic
		Carp	Ventricular strip	1	Biphasic
1964	Deck (1964)	Sheep	Purkinje fiber	1	Increasing
1972	Spear and Moore (1972)	Rat	Papillary muscle	1	Decreasing
		Rabbit	Papillary muscle	1	Constant
		Cat	Papillary muscle	1	Constant
		Guinea pig	Papillary muscle	1	Constant
		Frog	Trabeculae	1	Constant
1979	Dominguez and Fozzard (1979)	Sheep	Purkinje fiber	1	Increasing
1981	Rosen et al. (1981)	Cat	Trabeculae	1	Biphasic
		Dog	Purkinje fiber	1	Biphasic
1989	Solti et al. (1989)	Dog	Atria	1	CT increase
1996	Tavi et al. (1996)	Rat	Atria	1	Increasing
1996	Zabel et al. (1996b)	Rabbit	Ventricle	1	Delayed AT
1997	Reiter et al. (1997)	Rabbit	Left ventricle	2	Increasing[a]
1997	Zhu et al. (1997)	Dog	Ventricles	1	Constant AT
2003	Eijsbouts et al. (2003)	Rabbit	Atria	2	Decreasing
2003	Sung et al. (2003)	Rabbit	Left ventricle	2	Decreasing
2004	Sachse et al. (2004)	Rabbit	Papillary muscle	1	Biphasic

Abbreviations: CT: conduction time; AT: activation time.
[a]Increase of mean longitudinal conduction velocity only.

Biphasic. A biphasic relationship of strain and conduction velocity was reported for papillary muscle, atrial and ventricular strips of various species (Penefsky and Hoffman, 1963). In cat and terrapin, a maximal velocity was found at 100% strain corresponding to maximal force development. Conduction velocity increased in the low strain range (80–100%) and decreased in the high strain range (100% and above). Local activation times remained constant in the low strain range, but increased in the high strain range. All responses to strain were reversible.

Similarly, a biphasic-shaped profile with a maximal velocity for strain closely associated with maximal force was described for cat ventricular trabecular (Rosen et al., 1981), Purkinje fibers from young and adult canine (Rosen et al., 1981) and rabbit ventricular muscle (Sachse et al., 2004). In the studies of adult canine Purkinje fibers, the increase of strain from 75% to 115% relative to slack length in an exemplary fiber was associated with an increase of resting voltage from −85 to −70 mV and a decrease of upstroke velocity from 770 to 310 V/s.

Constant. An approximately constant conduction velocity, independent of strain, was reported in a study of papillary muscles from rabbit, cat and guinea pig and frog (Spear and Moore, 1972). The conduction velocity was determined by the ratio of distance between electrodes at the muscle ends and the latency between stimulus artifact and membrane depolarization. In the study of rabbit, strain varied between 76% and 110% with respect to maximal force development and conduction velocity was in general below 0.4 m/s.

Constant activation time (and thus velocity independent of strain) was also reported in a study of normal dogs and dogs with pacing-induced cardiomyopathy (Zhu et al., 1997). The measurements were carried out on the left ventricular anterior epicardium and tissue strain was increased by rapid infusion of intravenous saline. The amount of strain resulting from this injection was not measured.

Increasing. Increasing strain–velocity relationships were measured for Purkinje fibers of sheep (Deck, 1964; Dominguez and Fozzard, 1979). Increasing strain to 130% and 150% with respect to slack length resulted in 7.2% and 26% increase of conduction velocity (Dominguez and Fozzard, 1979). An increased conduction velocity for increased diastolic ventricular pressure (and thus increased strain) was found also in rat atria (Tavi et al., 1996). The increase of conduction velocity at increased pressure disappeared after application of the nsSAC blocker gadolinium.

Decreasing. A negative strain–velocity relationship was found for rat papillary muscle (Spear and Moore, 1972). In this study, strain varied between 87% and 110% with respect to maximal force development. The reduction of conduction velocity was approximately linear from 0.82 to 0.17 m/s.

A pacing site-dependent decrease of conduction velocity was reported for increased pressure in rabbit right atrium (Eijsbouts et al., 2003). Pacing at the cranial part of the crista terminalis resulted in no increase in conduction delays. However, pacing from the low right atrium revealed several lines of block oriented parallel to the major trabeculae and the crista terminalis. The same study investigated stimulus rate effects (4.1 versus 8 Hz) on the strain–conduction velocity relationship. The increase of rate reduced velocity in general.

In an optical mapping study of rabbit ventricles, conduction velocity decreased by 25% after increasing ventricular end-diastolic pressure from 0 to 30 mmHg (Sung et al., 2003). The pressure increase was associated with an anterior epicardial strain of 104% and 103% in muscle fiber and cross-fiber direction, respectively. Application of 200 μM streptomycin did not change the overall conduction velocity.

2.3. Review of computational studies

An overview of computational studies is given in Table 2. These studies were based on established models of electrical conduction in cardiac tissue extended with mathematical models of stretch-activated channels. Some of these studies included also models of strain-modulated tissue conductivity. Conduction is simulated in either cables, two-dimensional sheets or three-dimensional domains. The computational studies also showed differing relationships between strain and conduction velocity, which can be explained by the parameterization of models of stretch-activated channels and strain-modulated tissue conductivity.

A biphasic relationship between conductance of mechano-sensitive channels and conduction velocity was found in simulations of Purkinje fiber strands (Rice et al., 1998). The velocity increased for conductances in the range of $0-0.035\,\mathrm{pS/\mu m^2}$ and decreased rapidly for higher strain. Conductances above $0.045\,\mathrm{pS/\mu m^2}$ led to conduction block. Conduction block was explained by inactivation of fast sodium channels due to raised V_{rest} by opening of stretch-activated channels.

The same effect was suggested to underly slowed velocity in the high strain range (Mills et al., 2005), which was supported in a computational study of a guinea-pig myocyte strand (Sachse et al., 2006). In this study, the effect of raising diastolic transmembrane voltage by opening of stretch-activated non-selective cation channels and clamping of the diastolic transmembrane voltage was similar. In both cases, the increased V_{rest} from -90 to -60 mV led to reduction of upstroke velocity and conduction velocity.

Table 2
Computational studies of strain–conduction velocity relationships in cardiac tissue

Year	Authors and reference	Species	Tissue	Dim.	Relationship
1998	Rice et al. (1998)	Mammalian	Purkinje fiber	1	Biphasic
2000	Sachse et al. (2000)	Guinea pig	Ventricular	1,3	Variable[a]
2002	Sachse et al. (2002)	Guinea pig	Ventricular	2	Increasing
2004	Trayanova et al. (2004)	Mammalian	Ventricular	2	Variable[b]
2006	Sachse et al. (2006)	Guinea pig	Ventricular	1	Biphasic
2007	Kuijpers et al. (2007)	Human	Atrial	1	Decreasing
2007	Sachse et al. (2007)	Guinea pig	Ventricular	1	Biphasic

[a]Velocity is related to strain-modulated conductivity.
[b]Velocity decreased for cycle length shorter than 125 ms and increased otherwise.

Some computational studies indicated that the strain–conduction velocity relationship is effected by stimulus rate (Trayanova et al., 2004; Kuijpers et al., 2007; Sachse et al., 2007). In the high strain range, increased stimulus rate reduced current of the fast sodium channels, upstroke velocity and conduction velocity.

Further studies examined the effect of strain-modulated tissue conductivity on conduction velocity (Sachse et al., 2000, 2002; Kuijpers et al., 2007). Commonly, the underlying assumptions are that (1) the intercellular resistance associated to gap junctions is strain-independent and (2) the intercellular resistance associated to the cell interior is increased by strain.

In previous work, we suggested to describe strain-modulation of tissue conductivities as a tensor transformation based on the deformation gradient tensor $\boldsymbol{F}$, which is used in mechanics to derive various measures of strain (see Appendix A). Here, the conductivity tensor σ is transformed by stretch to the tensor σ_s (Sachse, 2004):

$$\sigma_s = \frac{1}{det\boldsymbol{A}} \boldsymbol{A}\sigma\boldsymbol{A}^T$$

with the second order weighting tensor $\boldsymbol{A}$ and the determinant operator det. The weighting tensor $\boldsymbol{A}$ is a function of the scalar weighting parameter θ:

$$\boldsymbol{A} = \boldsymbol{R}(\boldsymbol{I} + \theta(\boldsymbol{U} - \boldsymbol{I}))$$

with the unit tensor $\boldsymbol{I}$, the right stretch tensor $\boldsymbol{U}$ and rotation tensor $\boldsymbol{R}$ obtained by polar decomposition of the deformation gradient $\boldsymbol{F} = \boldsymbol{R}\boldsymbol{U}$. Reasonable choices of the weighting parameter θ are in the range $[0, 1]$. A weighting parameter $\theta = 0$ yields a conductivity independent of strain and thus that the associated resistor is increasing with strain (Assumption 1). A parameter $\theta = 1$ leads to $\boldsymbol{A} \equiv \boldsymbol{F}$ and a scaling of conductivity, which keeps the resistor between given points constant and independent of strain (Assumption 2). This setting would be appropriate if the gap junctions resistance is the dominant factor to intracellular conductivity.

The suggested transformation applies a single scaling parameter to describe the effect of strain on conductivity. While this approach is sufficient to account for the upper assumptions, extensions of the transformation such as anisotropic nonlinear scaling parameters might be useful to describe, e.g., extracellular conductivities. However, experimental data for parameterization of the transformation are currently sparse.

3. Methods

3.1. Experimental study

3.1.1. Papillary muscle preparation

The study was approved by the Institutional Animal Care and Use committee, University of Utah. New Zealand White rabbits (1–1.5 kg) were anti-coagulated with heparin (2500 USP units/kg) and anesthetized with intravenous administration of pentobarbital (25 mg/kg). The hearts were rapidly excised and moved to a dissection tray filled with a low calcium oxygenized bathing solution containing (in mM) 126 NaCl, 11 glucose, 4.4 KCl, 1.0 MgCl, 0.1 $CaCl_2$, 24 Hepes and 12.9 NaOH. After opening the right ventricle, a non-furcated papillary muscle with a diameter smaller than 1 mm and length between 3 and 5 mm was selected. The muscle was excised including the onset of the chordae tendinae. The harvested muscle was then stored in the solution at room temperature for 0.5 h. Afterwards, it was transferred to a horizontal flow-through chamber for mechanical fixation and measurement. Here, the papillary muscle was bathed with a similar solution as above. This solution (control) included 1 mM $CaCl_2$. The streptomycin perfusate consisted of the control solution being supplemented with 100 μM streptomycin. The temperature of each solution was $37.0 \pm 0.1\,^{\circ}C$. The muscle was left in the bathing solution for at least 0.5 h before the measurements began.

3.1.2. Experimental setup and protocol

The experimental setup and measurement protocol were similar as previously introduced (Sachse et al., 2004). In short, electrograms were recorded using a silver–silver-chloride electrode, which was positioned along the muscle surface using a software-controlled micro-manipulator. The software was developed in

LabVIEW 7.1 (National Instruments, TX). The locations for electrical measurements were calculated from the position of the distal and proximal muscle ends, which the user determined through positioning the recording electrode. The locations were digitally read into the computer. The software used the points to calculate 10 equidistant locations over the surface of the muscle. The location at the proximal end of the papillary muscle remained constant through the measurements, while the position at the distal end was reset manually as incremental strains were applied. This kept the measurement sites at the same position of the muscle as it was strained. Measurements started with a low strain of the muscle. Strain was increased incrementally every 2 min after taking electrical and force measurements and until conduction block occurred. Straining increments were either 100 or 200 μm. In some experiments, we continued the measurements after conduction block and reduced strain every 2 min until reaching the initial small strain.

The bathing solution was switched after taking a set of measurements. If the muscle was initially immersed in a streptomycin solution, it was changed to control and vice versa. The muscle was left in the new solution for at least 0.5 h before measurements were resumed, allowing for wash in or wash out of streptomycin.

Electrograms were low-pass filtered and recorded with a sampling frequency of 50 kHz. Force of contraction was measured using a force transducer (FORT10, World Precision Instruments Inc., FL) with a frequency of 1 kHz. Stimulus electrodes were of type silver–silver-chloride and were positioned at the proximal end of the papillary muscle. The electrical stimulus was biphasic with a duration shorter than 1 ms. In preliminary studies, we found that biphasic stimuli produced smaller artifacts in the electrogram than monophasic stimuli. The stimulus frequency was kept at 0.5 Hz during the measurements.

3.1.3. *Signal processing*

Acquired signals were analyzed offline using Matlab 7.2 (The Mathworks Inc., MA). All signals were digitally filtered using a third order Butterworth band pass (10–1000 Hz) and low pass (50 Hz) filter for the electrograms and force measurements, respectively. Each strain was normalized to the strain at maximal force development. The local activation time at each electrode position was defined as time of minimal temporal derivative in the extracellular unipolar electrogram in a time window after stimulation (Fig. 1) (Punske, 2000). The length of the stimulus artifact defined the start of the time window. Electrograms that were not biphasic or measured from proximal or distal sites were discarded when determining conduction velocity. Furthermore, only activation times that were a linear function of distance with a linear coefficient of $r^2 \geqslant 0.99$ were used to calculate conduction velocity (Fig. 2). The slope of the fitted line to the distance–activation time data determined the conduction velocity.

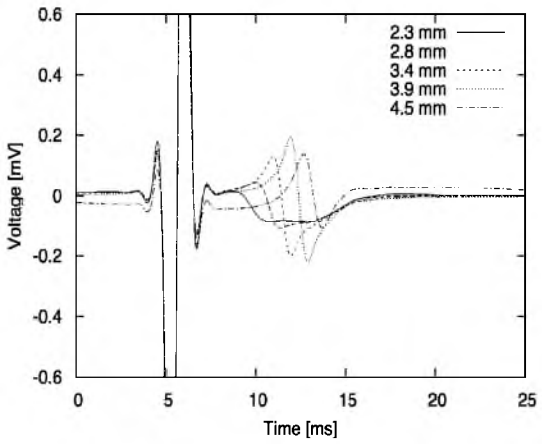

Fig. 1. Sample electrograms measured along a papillary muscle at different distances from the stimulus position. The distances range between 2.3 and 4.5 mm. The electrograms show truncated artifacts resulting from the biphasic stimuli starting at 4 ms with a duration of ≈ 3 ms. The local activation times are identified with a down-stroke in the electrogram. Activation times increase with distance from the stimulus position.

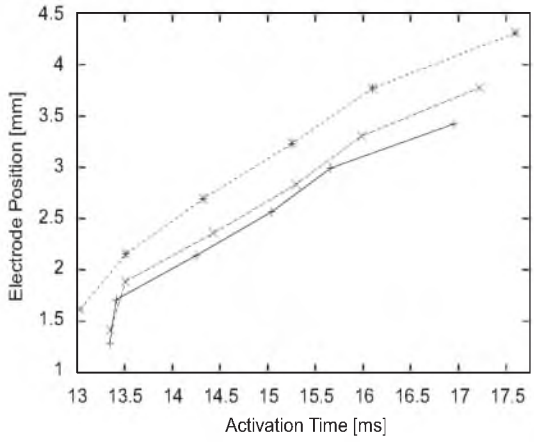

Fig. 2. Exemplary activation time–distance relationships extracted from electrograms. The plots show relationships for three measurements under different strain conditions. Conduction velocity v was calculated after selection of electrograms showing a linear activation time–distance relationship.

3.1.4. Data selection and statistics

Data sets with conduction velocity below 0.45 m/s at low strains were not included in statistical analysis as were data sets with peak velocity above 0.75 m/s. Several preparations showed velocities below 0.45 m/s, which is below the typical range for rabbit papillary muscle at physiological temperature (37.0 °C). The slow conduction might have been caused by partial gap junction closure due to damage during the extraction or mechanical fixation. Peak velocity above 0.75 m/s indicated the involvement of the fast conduction system such as Purkinje fibers with velocities in the range of 0.8 and 1.5 m/s at resting length and up to 2.2 m/s at high strain (Deck, 1964).

The mean strain–conduction velocity relationship in the rabbit papillary muscle was determined by a piecewise linear least squares fit. The fitting procedure yielded four continuous line segments specifying conduction velocities for strain in the ranges 80–90%, 90–100%, 100–110%, and between 110% and strain leading to conduction block.

Statistics on the conduction velocities for control and streptomycin measurements excluded conduction block; the strains at which conduction block occurred were compared separately. Statistical comparison was evaluated using Student's t-test where $p<0.05$ was considered to be significant.

3.2. Computational study

The modeling was performed as previously described (Sachse et al., 2007). In short, electrical conduction in rabbit right ventricular papillary muscle was simulated by a computational mono-domain model of a one-dimensional strand. The strand consists of 24 cardiac myocytes coupled by gap junctions with a resistance of 1.25 MΩ. The chosen resistance represents high electrical coupling and led to physiological conduction velocity at slack length of the strand. This intercellular resistance was defined as independent of strain and intracellular conductivity was neglected (see Section 2.3, Assumption 2).

Myocytes were represented by the Noble et al. model of guinea-pig ventricular cells (Noble et al., 1998). Currents through nsSACs were modeled by a Boltzmann-type relationship (Sachs, 1994) with reversal voltage of −30 mV and half-maximal conductance of 0.02 μS at strain $\lambda = 112.5\%$. The chosen reversal potential is in the range of potentials applied in related computational studies of −40 to −20 mV (Sachs, 1994), −25 to −20 mV (Zabel et al., 1996a) and −30 mV (Noble et al., 1998). Half-maximal conductance and associated strain were chosen to generate a membrane depolarization to −60 mV for strain $\lambda = 125\%$.

Simulations were carried out for various strain conditions of the papillary muscle. As a measure of strain the sarcomere length was varied between 1.68 and 2.52 μm. Here, a sarcomere length of 1.6, 2 and 2.5 μm represent

small strain ($\lambda = 80\%$), resting ($\lambda = 100\%$) and large strain condition ($\lambda = 125\%$) of the myocyte, respectively. Stimuli were applied at one end of the strand with a frequency of 0.5 Hz, which is identical as in our experimental studies. Simulation results after 15 stimuli were analyzed.

Conduction velocity was measured by detecting activation time of the 8th and 16th myocyte and assuming a myocyte length of 100 μm. Activation time was identified with the time at which the transmembrane voltage crosses −20 mV.

Activation duration was defined to characterize the upstroke of the transmembrane voltage. As a measure of activation duration, we chose the difference between the time $t_{90\%}$ at which the transmembrane voltages reaches 90% of resting voltage and the time $t_{-20\,\mathrm{mV}}$ at which the transmembrane voltage exceeds −20 mV:

$$\text{activation duration} = t_{-20\,\mathrm{mV}} - t_{90\%}.$$

Activation duration was measured at the 12th myocyte.

All calculations were performed in double precision floating point arithmetic. The system of ordinary differential equations underlying the myocyte model was solved with the forward Euler method using a time step of 1 μs (Press et al., 1992). Intercellular currents were updated every 1 μs.

4. Results

4.1. Experimental study

Strain–velocity relationship in control. Conduction velocity was measured at 6–10 different strains for each papillary muscle. The measurements started by applying small strain and continued with sequentially increasing strain. We acquired relationships in 17 papillary muscles. From these, 5 and 3 papillary muscles showed conduction velocities below 0.45 m/s at small strain or larger than 0.75 m/s, respectively. We did not include these data in further analysis. In the remaining nine experiments, peak and mean conduction velocities varied over a large range, but the individual relationships showed a similar progression. Examples of the measured strain–conduction velocity relationships for control are shown in Fig. 3. The averaged progression is depicted in Fig. 4. Conduction velocity increased with strain until a peak value of 59.8 ± 1.9 cm/s was reached at strain of ≈ 100%, which is the strain leading to maximal active force of contraction. The mean conduction velocity increased by 5% for 80–90% strain and by 12% for 80–100% strain. Strain beyond 100% caused the velocity to decrease until conduction block occurred at 118 ± 1.8% strain.

Strain–velocity relationship with streptomycin. With the same protocol as above, we measured the relationships in 14 papillary muscles bathed in a solution containing 100 μM streptomycin. Again, we excluded

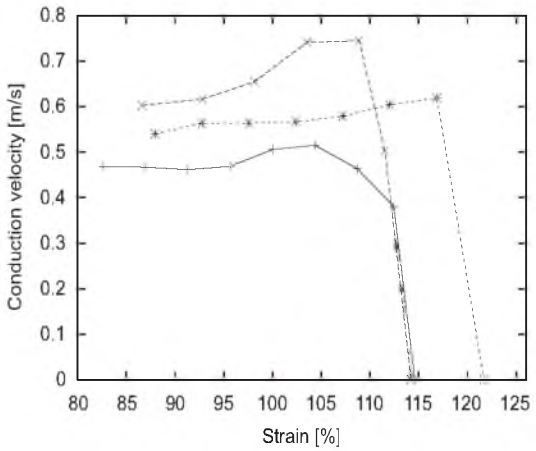

Fig. 3. Exemplary strain conduction velocity relationships in three papillary muscle preparations. Measurement data were marked with the symbols ×, ∗ and +. Conduction velocity shows an increase for small and middle strains. Conduction block was found at high strain. Range of conduction velocities can greatly differ between preparations.

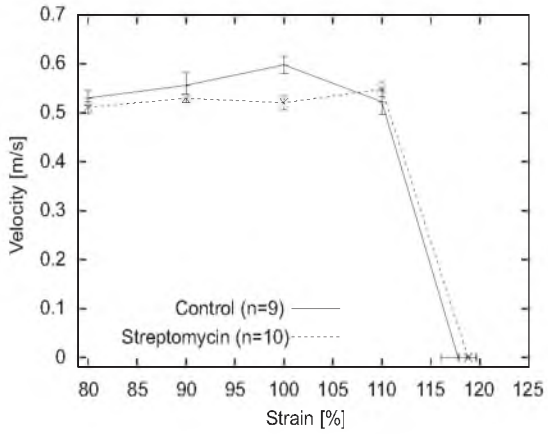

Fig. 4. Strain–conduction velocity relationship for control and after application of 100 μM streptomycin. Conduction velocity for control shows an increase in the range of 80–100% followed by a decrease before conduction block. Conduction velocity using streptomycin resulted in a smaller increase. However, conduction was blocked at similar strain. Vertical and horizontal bars indicate standard error of velocities and strains at block, respectively.

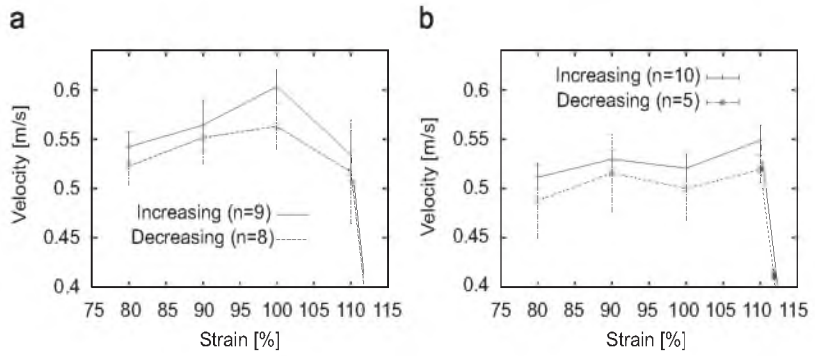

Fig. 5. Hysteresis of strain–conduction velocity relationship for (a) control and (b) after application of 100 μM streptomycin. In these experiments strain was increased until block and then decreased. Mean conduction velocity for each strain was larger during the increasing phase than the decreasing. For control, conduction velocity at 100% strain is 5 cm/s larger in the increasing versus decreasing phase.

data with conduction velocities below 0.45 m/s at small strain or larger than 0.75 m/s. The averaged progression is shown in Fig. 4. In the remaining 10 experiments, conduction velocity and progression were similar to control measurements for 80–90% strain. For 80–110% strain, the velocity was in general smaller and showed over this range only a moderate increase of 8%. Peak conduction velocity was 54.8 ± 1.5 cm/s at 110%, which is a statistical significant decrease of 9% in comparison to peak velocity in control. Conduction block occurred at 119 ± 0.8% strain with no statistically significant difference to control.

Block and hysteresis. We further investigated the mechanism of conduction block with an extension of the protocol described above. After block strain was incrementally reduced until the initial low strain configuration of the papillary muscle was reached. We found that the block is reversible by reducing strain (Fig. 5). The control measurements revealed hysteresis after block by comparing conduction velocities for increasing and decreasing strains. The average velocity and velocity at 100% strain decreased to 2.5% and 7.1%, respectively, from the increasing to decreasing strain in the control measurements. With streptomycin in the solution the decrease was reduced to 1.5% and 2.3% for average velocity and velocity at 100% strain, respectively.

4.2. Computational study

We performed computational simulations of mechano-electric effects with the one-dimensional model of cardiac tissue described above. Simulated resting voltage, maximal upstroke velocity and conduction velocity versus sarcomere length as a measure of strain are shown in Fig. 6. The strain–conduction velocity relationship was strongly dependent on involvement of nsSACs (Fig. 6a).

Without nsSAC currents, velocity was linearly related to strain. The conduction velocity at sarcomere length of 2.1 μm was 0.50 m/s. The velocity was 0.37 and 0.60 m/s at lowest and highest strain, respectively. A 10% increase in strain led to a 10% increase in velocity.

With nsSAC currents, velocity displayed a biphasic relationship to strain with a peak velocity of 0.62 m/s at sarcomere length of 2.275 μm (Fig. 6a). The velocity was 0.37 and 0.43 m/s at lowest and highest strain, respectively. For sarcomere lengths between 2 and 2.35 μm, nsSAC currents augmented the velocity in comparison to the velocity without nsSAC currents. Above 2.35 μm, nsSAC currents slowed conduction. With increasing strain the resting voltage decreased from −93 to −59 mV (Fig. 6b) and the maximal upstroke velocity decreased from 236 to 33 V/s (Fig. 6c). The simulations revealed a biphasic relationship between nsSAC currents and activation duration (Fig. 6d). The activation duration decreased with increasing nsSAC currents to a minimum of 0.527 ms at sarcomere length of 2.25 μm. For larger strain and increasing nsSAC, the activation duration increased.

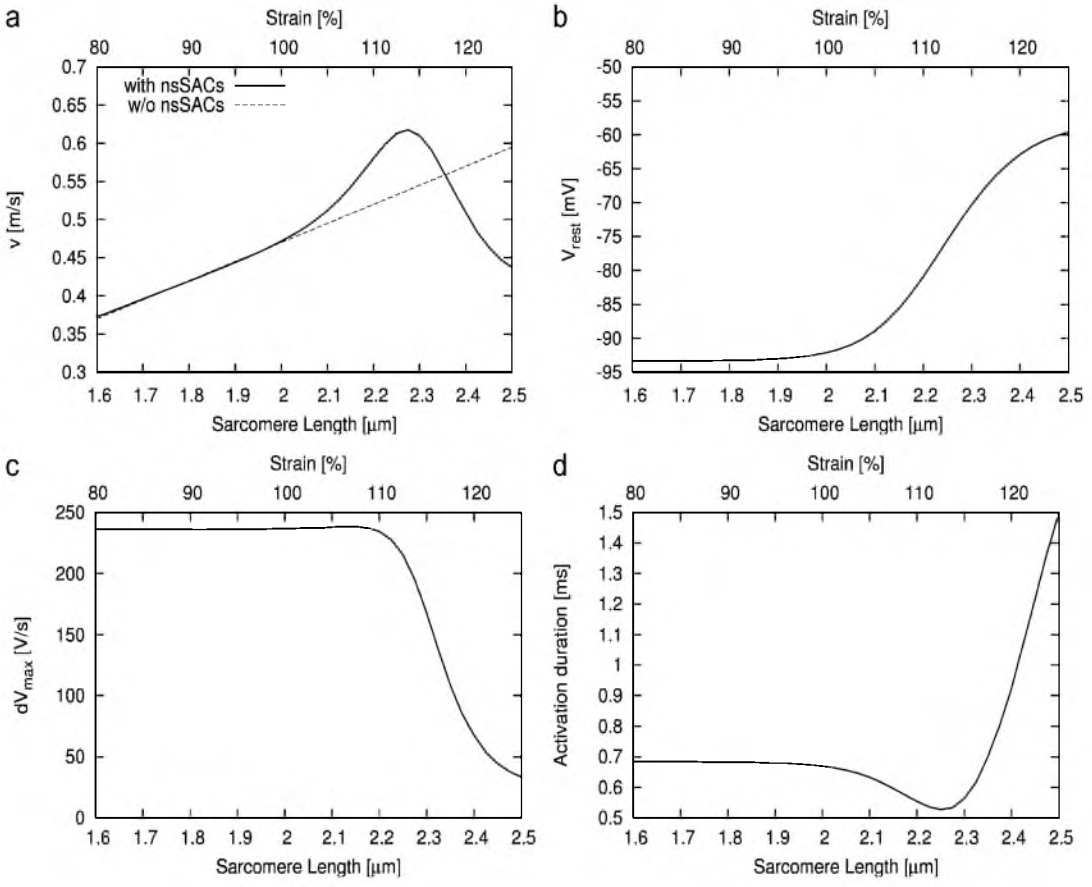

Fig. 6. Simulation of mechano-electric feedback in a one-dimensional model of cardiac tissue. Strain was quantified by sarcomere length. (a) The simulation yielded conduction velocity v as a function of sarcomere length. The strain–velocity relationship was determined with (solid) and without (dashed) involvement of nsSACs. Currents through nsSACs led to (b) resting voltage V_{rest} increasing with strain, (c) maximal upstroke velocity dV_{max} decreasing with strain and (d) a biphasic relationship between strain and activation duration.

5. Discussion and conclusions

5.1. Experimental studies

Our experimental data on rabbit papillary muscle supported the biphasic relationship of strain to conduction velocity, which has been previously reported in studies of mammals, reptiles and fishes (Penefsky and Hoffman, 1963; Rosen et al., 1981). We applied a wide range of strain from 80% to 120% with 100% referencing to strain of maximal force development. Smaller strains led to bending of the papillary muscle. The upper strain limit was decided by occurrence of conduction block. In the lower strain range (80–100%), the velocity was approximately linearly increasing with strain. In the higher strain range (above 100%), the velocity was decreasing with strain and eventually culminated in conduction block. The block occurred with a probability of 100% was reversible and associated with hysteresis of velocity.

The finding of a biphasic strain–conduction velocity relationship is in agreement with our computational studies. Biophysical mechanisms underlying the relationship are subsequently hypothesized (Section 5.2). Our discovery of conduction block at high strain is consistent with the occurrence of block reported for increased pressure in rabbit right atrium (Eijsbouts et al., 2003). In our studies, the block occurred at similar strain with or without streptomycin in the bathing solution. We conclude that the block is not related to activity of nsSACs. This conclusion is supported by our computational studies, which failed to reconstruct block with and without inclusion of nsSAC currents (Fig. 6a). Potential mechanisms underlying block are opening of the before mentioned K^+ stretch-modulated ion channels and mechano-sensitivity of gap junction channels. Opening of K^+ stretch-modulated ion channels would impose a larger electrical load on depolarizing myocytes potentially prohibitive for conduction. Closure of gap junction channels in the high strain range would prevent intercellular current flow and thus conduction. The latter hypothesis is supported by a recent single-channel and whole cell study of Cx46 hemi-channels (Bao et al., 2004), which showed that current through these hemi-channels is mechano-sensitive. However, Cx46 is not expressed in the heart and the mechano-sensitivity of cardiac connexins remains to be clarified.

Application of the nsSAC blocker streptomycin reduced peak velocity, shifted the associated strain to 110% from 100% in control and reduced the extent of hysteresis. Differences between control and streptomycin data were insignificant for strains between 80% and 90% as well as for strain at block. We conclude that under physiological conditions currents through nsSACs are contributing to peak velocity and the initial phase of subsequent decreasing of velocity. The conclusion is supported by our computational studies, which showed that nsSAC currents boost and reduce conduction velocity for moderate and large strain, respectively (Fig. 6a).

Furthermore, the nsSAC currents appear to be responsible for hysteresis. Under physiological conditions, the opening of nsSACs results in inward currents of sodium and calcium and outward current of potassium. We speculate that in the long-term these currents change intracellular ion concentrations, which directly or indirectly reduce conduction velocity. The mechanism could involve the electrogenic sodium–calcium exchanger (NCX). Increased concentrations of intracellular calcium increases the transfer of calcium out of and sodium into the cell by NCX. Assuming that the calcium concentration is sub-acutely raised, a persisting NCX activity could depolarize the membrane and cause sodium channel inactivation.

Limitations. The measured velocities showed a high inter-preparation variability (Fig. 3). Several reasons can account for this variability: Firstly, several preparations showed very large velocities up to 1.3 m/s, which indicated involvement of the fast conduction system. We did not include data from experiments with peak velocity larger than 0.75 m/s in our analysis. However, we cannot exclude the possibility that excitation was partially carried by the fast conduction system in some of our preparations. Secondly, the diameters of the preparations were inhomogeneous. Velocity in a strand preparation is moderately dependent on its diameter (Roth, 1991). A strand with radius of 0.2 mm has an $\approx 8\%$ larger velocity than with 0.6 mm radius. Thirdly, the shape of the preparations was inhomogeneous. Some muscles had uniform circular cross-sections, others were slightly tapered toward the tendon. This shape variation might affect conduction velocity, but to what extent is unclear. Despite the high inter-preparation variability the biphasic relationship was consistently found in our measurements.

The application of streptomycin to block nsSACs in tissue and whole heart preparations has been questioned in several studies (Lamberts et al., 2002; Sung et al., 2003; Cooper and Kohl, 2005; Garan et al., 2005). Application of streptomycin in sino-atrial node tissue from guinea pigs and mice did not eliminate strain related changes of the chronotropic beat rate (Cooper and Kohl, 2005). Application of streptomycin did not alter the frequency of ventricular fibrillation in a study of commotio cordis in pig heart (Garan et al., 2005) and did not affect electrophysiological changes related to increased ventricular filling in a study of isolated rabbit heart (Sung et al., 2003). Conversely, arrhythmias were suppressed in the presence of streptomycin when whole rat hearts were exposed to increased ventricular pressure (Salmon et al., 1997). The slow inotropic response of rat cardiac myocytes and tissue was reduced by streptomycin (Calaghan and White, 2004). Also, in myocyte preparations, nsSACs have been reportedly blocked by streptomycin (Belus and White, 2003). In our hands, the application of 100 μM streptomycin strongly affected the strain-modulation of conduction velocity in a manner compatible to the subsequently described hypothesis to explain this mechano-electric feedback phenomenon. However, the degree of nsSAC block by streptomycin remains unknown. In our studies, streptomycin sulphate was used. The upper concentration of the nsSAC blocker refers to the single streptomycin molecule (White, 2006).

Our measurements were carried out with isometric condition of the tissue, while under physiological conditions cardiac muscle undergoes marked contractions during each beat. Isometry is an approximation of physiological conditions, where conduction occurs at the end of diastole while the heart is almost in a steady mechanical state. The condition was used in previous studies of strain–conduction velocity relationships in papillary muscle, Purkinje fibers and tissue strips. With our protocol, measurements were taken every 2 min and immediately afterwards strain was increased or decreased. Thus, our measurements represent only steady state conditions and transient effects were neglected.

5.2. *Computational studies*

Our simulations reconstructed a biphasic relationship of strain and conduction velocity similarly as revealed in our experimental studies of rabbit papillary muscle. The biphasic relationship resulted from the combined effects of two factors of mechano-electric feedback: nsSACs and strain-modulated intercellular conductivity (Fig. 7). Our choice of strain-independent resistance led to linearly increasing strain–conduction velocity relationships for all strains (Fig. 6a). Currents through nsSACs had varied effects. At moderate strain, nsSAC currents depolarized the membrane in such a manner that time to activation was reduced despite upstroke velocity was identical as for small strains. At large strain, the increased depolarization of the membrane led to inactivation of the fast sodium channels and their availability was strongly reduced. This reduction diminished upstroke velocity of the transmembrane voltage and slowed conduction.

Our computational results are in qualitative agreement with previous experimental work with various tissues and species (Penefsky and Hoffman, 1963; Rosen et al., 1981; Sachse et al., 2004) as well as with computational studies on mammalian Purkinje fibers (Rice et al., 1998) and mammalian myocardial strips (Trayanova et al., 2004). Our findings are not in complete agreement with a computational study of strain–conduction velocity relationships in human atrial tissue (Kuijpers et al., 2007). This study indicated a generally decreasing relationship for strain $\lambda \geqslant 100\%$ in accordance with studies in dog and rabbit atrial tissue (Solti et al., 1989; Eijsbouts et al., 2003). In part, the differences between the computational studies can be explained by different parameterization of nsSACs. The activation of nsSAC currents was shifted to smaller strains and conductances were sufficiently large to block conduction at high strain by inactivation of the fast sodium channels. Further differences are related to their definition of strain-modulated intercellular conductivity leading to constant or linearly decreasing strain–velocity relationships.

The computational studies with and without inclusion of nsSAC currents did not reconstruct block of conduction, which occurred in our experiments with a probability of 100% with and without application of 100 μM streptomycin for extreme strain (Fig. 4). The simulations demonstrated that nsSAC currents can boost or lower conduction velocity, but with the given parameterization the currents were insufficient to depolarize the membrane to such an extent that cells were inexcitable and conduction was blocked. In principle, this would have been possible by increasing nsSAC conductivity. However, the occurrence of block in our

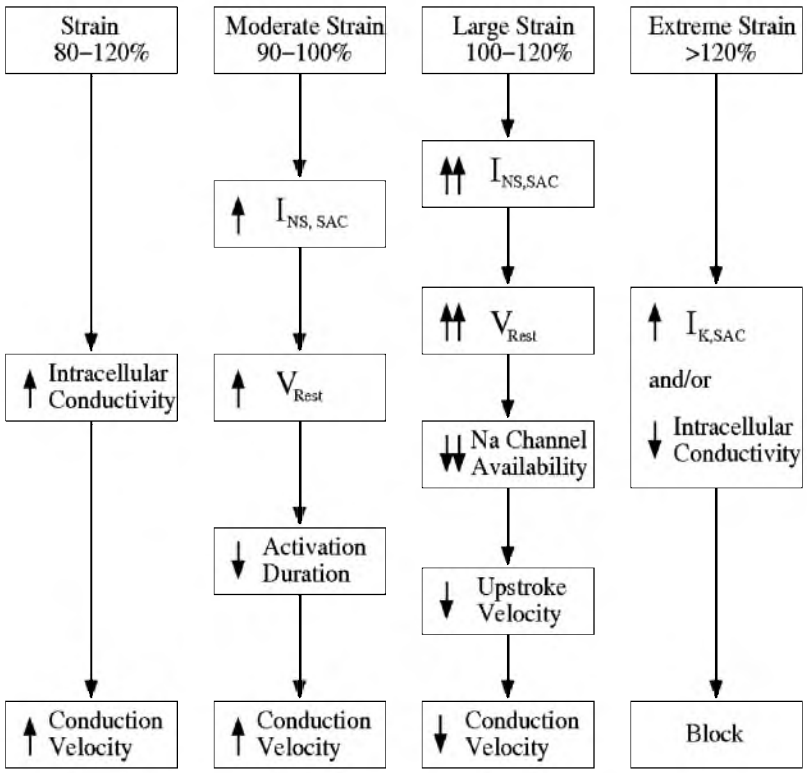

Fig. 7. Hypotheses for mechanisms of strain–conduction velocity relationships in ventricular tissue. We suggest that four different mechanisms are relevant. Two of these, strain-modulated conductivity and depolarizing nsSAC currents $I_{NS,SAC}$ for moderate strain, lead to positive strain–velocity relationships. Depolarizing currents $I_{NS,SAC}$ at large strain underly the negative relationship. A less understood mechanisms is suggested to be responsible for block.

experimental studies in presence of streptomycin indicates that such an approach would be inappropriate. Currently, experimental data explaining conduction block at extreme strain are sparse. We suggest that studies of mechanical modulation of conduction and intercellular resistance in myocyte pairs will help to gain insights in biophysical mechanisms of block.

Limitations. With our computational studies we aimed at a qualitative reconstruction of strain–conduction velocity relationships. We did not apply more detailed conduction models such as three-dimensional bidomain models, which we have used before for reconstruction of wave propagation in papillary muscle (Sachse et al., 2005). Also, we did not attempt a quantitative reconstruction of the experimental data.

We suggest that optimized descriptions of nsSACs and integration of these in an electrophysiological model of rabbit myocytes will improve the reconstruction of our experimental data. We applied a Boltzmann-type relationship of nsSAC currents to strain (Sachs, 1994). Various other descriptions of nsSACs have been suggested (Rice et al., 1998; Noble et al., 1998; Zeng et al., 2000). Remarkable differences between the guinea-pig model of Noble et al. (1998) applied in our study and the model of rabbit ventricular myocytes of Puglisi and Bers (2001) can be found for resting transmembrane voltage and upstroke velocity. Both are important factors contributing to the strain–conduction velocity relationship (Section 2.1).

The steepness of the simulated strain–velocity relationship in the low strain range is about twice of the steepness of the measured data. Thus, the assumed strain-independence of intercellular resistance (Section 2.3, Assumption 2) appears to be an oversimplification and an extreme choice. An intermediate behavior would reduce the large effect of strain on conduction velocity in the low strain range.

5.3. Comparison with studies of atria and ventricles

In our studies on papillary muscles we applied one-dimensional strain in the muscle's long axis direction, which is also the myocytes' long axis direction. Assuming volume preservation of cardiac tissue and transversal isotropic tissue properties, increased straining in fiber direction λ_{fiber} will lead to reduced strain in the two orthogonal cross-fiber directions $\lambda_{\text{cross-fiber}}$:

$$\lambda_{\text{cross-fiber}} = \sqrt{\frac{1}{\lambda_{\text{fiber}}}}.$$

Similar straining conditions are commonly applied in studies of stretch-activated currents in isolated myocytes.

The straining condition is different in studies of atria or ventricles, in which strain is modified by setting cavity pressure or volume (Solti et al., 1989; Tavi et al., 1996; Zabel et al., 1996a; Reiter et al., 1997; Zhu et al., 1997; Eijsbouts et al., 2003; Sung et al., 2003). In these studies, increasing pressure or volume caused an increase of strain in fiber and epicardial cross-fiber direction, which presumably is associated with a reduction of strain in the orthogonal direction. Ventricular filling studies indicated that the resulting strains in fiber and epicardial cross-fiber direction are significantly smaller than strain applied in studies on papillary muscle and Purkinje fibers (Sung et al., 2003).

5.4. Summary

Major features in our experimental and computational studies of ventricular tissue were the biphasic strain–conduction velocity relationship and block at extreme strain. Our computational studies supported previous work done by us and others showing that this relationship is associated with a positive strain–resting voltage and negative strain–maximal upstroke velocity relationship at cellular level. Our computational studies did not reconstruct block at extreme strain and further experimental studies are necessary to gain data on this effect.

A summary of our hypotheses to explain the biphasic relationship and block is given in Fig. 7. We propose four partially cooperative mechanisms which are associated to specific strain ranges:

- Over the complete strain range: strain-modulated conductivity causes a linear positive relationship.
- Moderate strain: nsSAC currents lead to a positive relationship by reduction of activation duration.
- Large strain: nsSAC currents yield a negative relationship by sodium channel inactivation.
- Extreme strain: block results from an unknown mechanism, potentially currents through stretch-activated potassium channels and/or closure of gap junction channels.

Only the first three hypothesized mechanisms have been supported by experimental and computational studies.

Our hypotheses might explain uni-axially applied strain–conduction velocity relationships in other types of cardiac tissue such as Purkinje fibers and trabeculae. However, the hypotheses necessitate adjustment to reconstruct pressure or volume related changes of velocity in atria and ventricles.

Acknowledgments

This work was funded by the Richard A. Harrison and Nora Eccles Fund for Cardiovascular Research and awards from the Nora Eccles Treadwell Foundation.

Editor's note

Please see also related communications in this issue by Zhang et al. (2008) and Loiselle et al. (2008).

Appendix A. Measures of strain

Strain tensors. Different descriptions of strain are found in mechanics to specify deformation of a material (Bathe, 1982). For example, in continuum mechanics tensors of second order, e.g. the Cauchy strain tensor $\boldsymbol{C}$ and the Lagrange strain tensor $\boldsymbol{E}$, are applied to quantify the deformation. These tensors are derived from the deformation gradient tensor $\boldsymbol{F}$, which can be defined by differentiating the coordinates ${}^{t}\boldsymbol{x}({}^{0}\boldsymbol{x}, t)$ with respect to the reference configuration coordinates ${}^{0}\boldsymbol{x}$ in a cartesian system:

$$ {}^{t}_{0}\boldsymbol{X} = \left[\frac{\partial {}^{t}x_i}{\partial {}^{0}x_j}\right] = \begin{pmatrix} \frac{\partial {}^{t}x_1}{\partial {}^{0}x_1} & \frac{\partial {}^{t}x_1}{\partial {}^{0}x_2} & \frac{\partial {}^{t}x_1}{\partial {}^{0}x_3} \\ \frac{\partial {}^{t}x_2}{\partial {}^{0}x_1} & \frac{\partial {}^{t}x_2}{\partial {}^{0}x_2} & \frac{\partial {}^{t}x_2}{\partial {}^{0}x_3} \\ \frac{\partial {}^{t}x_3}{\partial {}^{0}x_1} & \frac{\partial {}^{t}x_3}{\partial {}^{0}x_2} & \frac{\partial {}^{t}x_3}{\partial {}^{0}x_3} \end{pmatrix}. $$

One-dimensional strain. One-dimensional strain λ is commonly described by the ratio of length under load l to resting length L:

$$ \lambda = \frac{l}{L}. $$

Here, strain is unit-less and has a value of 1 if no loads are applied. We used this notation for specifying strain at cellular level.

In this work, we commonly quantified strain in cardiac tissue with reference to strain for maximal force development and in percentage:

$$ \lambda_{\mathrm{F,max}} = \frac{l}{L_{\mathrm{F,max}}} 100\%. $$

Thus, a strain of 100% would correspond to peak force development. The choice is motivated by simple accessibility of force in studies of papillary muscle, trabeculae, atrial and ventricular strips, and Purkinje fibers.

References

Bao, L., Sachs, F., Dahl, G., 2004. Connexins are mechanosensitive. Am. J. Physiol. Cell Physiol. 287, C1389–C1395.

Bathe, K.-J., 1982. Finite Element Procedures in Engineering Analysis. Prentice-Hall, Englewood Cliffs, NJ.

Belus, A., White, E., 2003. Streptomycin and intracellular calcium modulate the response of single guinea-pig ventricular myocytes to axial stretch. J. Physiol. 15 (546), 501–509.

Calaghan, S.C., 2007. Stretch and caveolae. In: Proceedings of the Cardiac MEF and Arrhythmias. Oxford, pp. 24–25.

Calaghan, S., White, E., 2004. Activation of $Na^{+}-H^{+}$ exchange and stretch-activated channels underlies the slow inotropic response to stretch in myocytes and muscle from the rat heart. J. Physiol. 559 (1), 205–214.

Cooper, P.J., Kohl, P., 2005. Species- and preparation-dependence of stretch effects on sino-atrial node pacemaking. Ann. N.Y. Acad. Sci. 1047, 324–335.

Deck, K.A., 1964. Änderungen des Ruhepotentials und der Kabeleigenschaften von Purkinje-Fäden bei der Dehnung. Pflügers Arch. 280, 131–140.

Dominguez, G., Fozzard, H.A., 1979. Effect of stretch on conduction velocity and cable properties of cardiac Purkinje fibers. Am. J. Physiol. 237 (3), C119–C124.

Eijsbouts, S.C.M., Majidi, M., van Zandvoort, M., Allessie, M.A., 2003. Effects of acute atrial dilation on heterogeneity in conduction in the isolated rabbit heart. J. Cardiovasc. Electrophysiol. 14, 269–278.

Franz, M.R., Bode, F., 2003. Mechano-electrical feedback underlying arrhythmias: The atrial fibrillation case. Prog. Biophys. Mol. Biol. 82 (1–3), 163–174.

Garan, A.R., Maron, B.J., Wang, P.J., III, N.A.E., Link, M.S., 2005. Role of streptomycin-sensitive stretch-activated channel in chest wall impact induced sudden death (commotio cordis). J. Cardiovasc. Electrophysiol. 16(4), 433–438.

Hsieh, J.C., Chen, S.-A., Tai, C.-J., Li, J. K.-J., 1999. The influences of cardiac mechano-electrical feedback on action potential duration. In: Conference Proceedings of IEEE Engineering Medicine and Biology, vol. 1, p. 142.

Kohl, P., Cooper, P.J., Holloway, H., 2003. Effects of acute ventricular volume manipulation on in situ cardiomyocyte cell membrane configuration. Prog. Biophys. Mol. Biol. 82 (1–3), 222–227.

Kuijpers, N., Ten Eikelder, H., Bovendeerd, P., Verheule, S., Arts, T., Hilbers, P., 2007. Mechano-electric feedback leads to conduction slowing and block in acutely dilated atria: a modeling study of cardiac electromechanics. Am. J. Physiol. Heart Circ. Physiol. 292 (6), H2832–H2853.

Lamberts, R.R., Van Rijen, M.H., Spikema, P., Fransen, P., Sys, S.U., Westerhof, N., 2002. Coronary perfusion and muscle lengthening increase cardiac contraction: different stretch-triggered mechanisms. Am. J. Physiol. Heart Circ. Physiol. 283 (4), H1512–H1522.

Li, X.T., Dyachenko, V., Zuzarte, M., Putzke, C., Preisig-Muller, R., Isenberg, G., Daut, J., 2006. The stretch-activated potassium channel TREK-1 in rat cardiac ventricular muscle. Cardiovasc. Res. 69 (1), 86–97 ePub October 24, 2005.

Loiselle, D.S., Crampin, E.J., Niederer, S.A., Smith, N.P., Barclay, C.J., 2008. Energetic consequences of mechanical loads, Prog. Biophys. Mol. Biol. 97, 348–366.

Maroto, R., Raso, A., Wood, T.G., Kurosky, A., Martinac, B., Hamill, O.P., 2005. TRPC1 forms the stretch-activated cation channel in vertebrate cells. Nat. Cell. Biol. 7 (2), 105–107.

Mills, R.W., Narayan, S.M., McCulloch, A.D., 2005. The effects of wall stretch on ventricular conduction and refractoriness in the whole heart. In: Kohl, P., Franz, M.R., Sachs, F. (Eds.), Cardiac Mechano-Electric Feedback and Arrhythmias. Elsevier Saunders, pp. 127–136.

Niu, W., Sachs, F., 2003. Dynamic properties of stretch-activated K^+ channels in adult rat atrial myocytes. Prog. Biophys. Mol. Biol. 82 (1–3), 121–135.

Noble, D., Varghese, A., Kohl, P., Noble, P., 1998. Improved guinea-pig ventricular cell model incorporating a diadic space, I_{Kr} and I_{Ks}, and length- and tension-dependend processes. Can. J. Cardiol. 14 (1), 123–134.

Penefsky, Z.J., Hoffman, B.F., 1963. Effects of stretch on mechanical and electrical properties of cardiac muscle. Am. J. Physiol. 204 (3), 433–438.

Press, W.H., Teukolsky, S.A., Vetterling, W.T., Flannery, B.P., 1992. Numerical Recipes in C, second ed. Cambridge University Press, Cambridge, New York, Melbourne.

Puglisi, J.L., Bers, D.M., 2001. LabHEART: an interactive computer model of rabbit ventricular myocyte ion channels and Ca transport. Am. J. Physiol. 281, C2049–C2060.

Punske, B.B., 2000. Determining the local time of activation from the unipolar electrogram: new methods, new challenges. J. Cardiovasc. Electrophysiol. 11, 1129–1131.

Reiter, M.J., Landers, M., Zetelaki, Z., Kirchhof, C.J.H., Allessie, M.A., 1997. Electrophysiological effects of accute dilation in the isolated rabbit heart. Circulation 96, 4050–4056.

Rice, J.J., Winslow, R.L., Dekanski, J., McVeigh, E., 1998. Model studies of the role of mechano-sensitive currents in the generation of cardiac arrhythmias. J. Theor. Biol. 190, 295–312.

Riemer, T.L., Tung, L., 2003. Stretch-induced excitation and action potential changes of single cardiac cells. Prog. Biophys. Mol. Biol. 82 (1–3), 97–110.

Rosen, M.R., Legato, M.J., Weiss, R.M., 1981. Developmental changes in impulse propagation in the canine heart. Am. J. Physiol. 240, H546–H554.

Roth, B.J., 1991. Action potential propagation in a thick strand of cardiac muscle. Circ. Res. 68, 162–173.

Ruknudin, A., Sachs, F., Bustamante, J.O., 1993. Stretch-activated ion channels in tissue-cultured chick heart. Am. J. Physiol. Heart Circ. Physiol. 264 (33), H960–H972.

Sachs, F., 1994. Modeling mechanical-electrical transduction in the heart. In: Mow, C., Guilak, F., Tran-Son-Tay, R., Hochmuth, R.M. (Eds.), Cell Mechanics and Cellular Engineering. Springer, New York, pp. 308–328.

Sachs, F., 2004. Mechanoelectric transduction. In: Zipes, D.P., Jalife, J. (Eds.), Cardiac Electrophysiology. From Cell to Bedside, fourth ed. W.B. Saunders Company, Philadelphia, pp. 96–102 (Chapter 11).

Sachse, F.B., 2004. Computational cardiology: modeling of anatomy, electrophysiology, and mechanics. In: Lecture Notes in Computer Science, vol. 2966. Springer, Heidelberg.

Sachse, F.B., Seemann, G., Riedel, C., Werner, C.D., Dössel, O., 2000. Modeling of the cardiac mechano-electrical feedback. Int. J. Bioelectromagn. 2 (2).

Sachse, F.B., Seemann, G., Riedel, C., 2002. Modeling of cardiac excitation propagation taking deformation into account. In: Proceedings of BIOMAG 2002, pp. 839–841.

Sachse, F.B., Steadman, B.W., Bridge, J.H.B., Punske, B.B., Taccardi, B., 2004. Conduction velocity in myocardium modulated by strain: measurement instrumentation and initial results. In: Conference Proceedings of IEEE Engineering Medicine and Biological Society, vol. 5, pp. 3593–3596.

Sachse, F.B., Seemann, G., Taccardi, B., 2005. Insights into electrophysiological studies with papillary muscle by computational models. In: Franji, A.F., Radeva, P.I., Santos, A., Hernandez, M. (Eds.), Lecture Notes in Computer Science, vol. 3504. Springer, Berlin, pp. 216–225.

Sachse, F.B., Seemann, G., Taccardi, B., 2006. Relationship of strain and conduction velocity in cardiac muscle in the high strain range. In: Biophys. J. (Annual Meeting Abstracts), p. 2644.

Sachse, F.B., Hunter, G.A.M., Weiss, D.L., Seemann, G., 2007. A framework for modeling of mechano-electrical feedback mechanisms of cardiac myocytes and tissues. In: Conference Proceedings of IEEE Engineering Medicine and Biological Society, vol. 1, pp. 160–163.

Salmon, A.H., Mays, J.L., Dalton, G.R., Jones, J.V., Levi, A.J., 1997. Effect of streptomycin on wall-stress-induced arrhythmias in the working rat heart. Cardiovasc. Res. 34 (3), 493–503.

Solti, F., Vecsey, T., Kékesi, V., Juhász-Nagy, A., 1989. The effect of atrial dilation on the genesis of atrial arrhythmias. Cardiovasc. Res. 23, 882 886.

Spear, J.F., Moore, E.N., 1972. Stretch-induced excitation and conduction disturbances in the isolated rat myocardium. J. Electrocardiol. 5 (1), 15 24.

Sung, D., Mills, R.W., Schettler, J., Narayan, S.M., Omens, J.H., McCulloch, A.D., 2003. Ventricular filling slows epicardial conduction and increases action potential duration in an optical mapping study of the isolated rabbit heart. J. Cardiovasc. Electrophysiol. 14 (7), 739 749.

Tavi, P., Laine, M., Weckström, M., 1996. Effect of gadolinium on stretch-induced changes in contraction and intracellularly recorded action- and after potentials of rat isolated atrium. Br. J. Pharmacol. 118, 407 413.

Trayanova, N., Li, W., Eason, J., Kohl, P., 2004. Effect of stretch-activated channels on defibrillation efficacy. Heart Rhythm 1 (1), 67 77.

White, E., 2006. Mechanosensitive channels: therapeutic targets in the myocardium? Curr. Pharm. Des. 12 (28), 3645 3663.

White, E., Guennec, J.-Y.L., Nigretto, J.M., Gannier, F., Argibay, J.A., Garnier, D., 1993. The effects of increasing cell length on auxotonic contractions: membrane potential and intracellular calcium transients in single guinea-pig ventricular myocytes. Exp. Physiol. 78 (1), 65 78.

Zabel, M., Koller, B.S., Sachs, F., Franz, M.R., 1996a. Stretch-induced voltage changes in the isolated beating heart: importance of the timing of stretch and implications for stretch-activated ion channels. Cardiovasc. Res. 32, 120 130.

Zabel, M., Portnoy, S., Franz, M.R., 1996b. Effect of sustained load on dispersion of ventricular repolarization and conduction time in the isolated intact rabbit heart. J. Cardiovasc. Electrophysiol. 7, 9 16.

Zeng, T., Bett, G.C.L., Sachs, F., 2000. Stretch-activated whole cell currents in adult rat cardiac myocytes. Am. J. Physiol. 278, H548 H557.

Zhang, Y.H., Youm, J.B., Sung, H.K., Lee, S.H., Ryu, S.Y., Lee, S.-H., Ho, W.-K., Earm, Y.E., 2000. Stretch-activated and background non-selective cation channels in rat atrial myocytes. J. Physiol. 523 (3), 607 619.

Zhang, Y., Sekar, R.B., McCulloch, A.D., Tung, L., 2008. Cell cultures as models of cardiac mechanoelectric feedback. Prog. Biophys. Mol. Biol. 97, 367 382.

Zhu, W.X., Johnson, S.B., Brandt, R., Burnett, J., Packer, D.L., 1997. Impact of volume loading and load reduction on ventricular refractoriness and conduction properties in canine congestive heart failure. J. Am. Coll. Cardiol. 30 (3), 825 833.

3. STRAIN TRANSFER IN VENTRICULAR CARDIOMYOCYTES TO THEIR TRANSVERSE TUBULAR SYSTEM REVEALED BY SCANNING CONFOCAL MICROSCOPY

Reprinted with permission from Biophysical Journal, Volume 100 May 2011, L53-L55

Biophysical Journal Volume 100 May 2011 L53–L55

Strain Transfer in Ventricular Cardiomyocytes to Their Transverse Tubular System Revealed by Scanning Confocal Microscopy

Thomas G. McNary,[†‡] John H. B. Bridge,[†§] and Frank B. Sachse[†‡*]
[†]Nora Eccles Harrison Cardiovascular Research and Training Institute, [‡]Department of Bioengineering, and [§]School of Medicine, University of Utah, Salt Lake City, Utah

ABSTRACT The transverse tubular system (t-system) is a major site for signaling in mammalian ventricular cardiomyocytes including electrical signaling and excitation-contraction coupling. It consists of membrane invaginations, which are decorated with various proteins including mechanosensitive ion channels. Here, we investigated mechanical modulation of the t-system. By applying fluorescent markers, three-dimensional scanning confocal microscopy, and methods of digital image analysis, we studied isolated ventricular cardiomyocytes under different strains. We demonstrate that strain at the cellular level is transmitted to the t-system, reducing the length and volume of tubules and altering their cross-sectional shape. Our data suggest that a cellular strain of as little as 5% affects the shape of transverse tubules, which has important implications for the function of mechanosensitive ion channels found in them. Furthermore, our study supports a prior hypothesis that strain can cause fluid exchange between the t-system and extracellular space.

Received for publication 21 January 2011 and in final form 24 March 2011.

*Correspondence: fs@cvrti.utah.edu

Mammalian ventricular myocytes exhibit a transverse tubular system (t-system), which consists of membrane invaginations (1). Geometry and morphology of the t-system were found to be dependent on species and cell type (2). The t-system is an important site for excitation-contraction coupling and essential for rapid electrical signaling from the outer sarcolemma into the cell interior. Recent interest in the t-system has been renewed by studies demonstrating that transverse tubules (t-tubules) are less dense and their arrangement is disorganized in diseased ventricular cardiomyocytes (3,4).

It has been suggested that t-tubular loss reduces the efficiency of cardiac excitation-contraction coupling (5). It has also been suggested that mechanical deformation of the t-system can contribute to fluid exchange between it and the interstitial space (2,6). Such a pumping mechanism would support transport of nutrients, metabolites, and ions into the myocyte. Any t-system deformation may contribute to mechanical modulation of ion channels. Mechanosensitive ion channels found in the t-system include stretch-activated transient receptor potential cation channels (TRPC6) and stretch-modulated inward rectifier potassium channels (Kir2.3) (7).

The aim of this study was to characterize the transfer of strain at cellular level to the t-system. The study is based on our previous work, which applied three-dimensional scanning confocal microscopy on living isolated cardiomyocytes to characterize geometrical features of the t-system (2). We found that the rabbit t-system rarely exhibits longitudinal tubules. We demonstrated flattening of t-tubule cross sections and alignment of their short axis with the long axis of myocytes. We suggested that the flattening is related to the myocytes being at a slack length and is altered when they shorten or lengthen.

Using this experimental and analytical approach, we studied mechanical deformation of the t-system of myocytes. Strain was applied statically by longitudinal stretching of the myocytes. We hypothesized that 1), cellular strain is transmitted to the t-system; and 2), mechanical deformation of myocytes contributes to fluid transport between the t-system cavities and extracellular space. We tested these hypotheses by imaging and comparison of geometrical features of t-tubules in quiescent myocytes at rest and during static strain.

The protocol used for isolating rabbit myocytes is described in the Supporting Material. The myocytes were transferred to an imaging chamber, suffused with a membrane-impermeable dextran conjugated to fluorescent dye (Alexa 488; Invitrogen, Carlsbad, CA), and imaged using a LSM 5 Duo confocal microscope (Carl Zeiss, Jena, Germany). The setup for imaging and straining of myocytes is shown in Fig. S1 in the Supporting Material. Exemplary images obtained from a myocyte before and during strain are shown in Fig. 1.

The image stacks were deconvolved and corrected for background signals and depth-dependent attenuation (8). Longitudinal spacing of t-tubules, Δ, was determined by maxima in Fourier spectra of the three-dimensional images. Strain was defined as $\Delta_{Strained}/\Delta_{Unstrained}$ with $\Delta_{Strained}$ and

Editor: Andrew McCulloch.

doi: 10.1016/j.bpj.2011.03.046

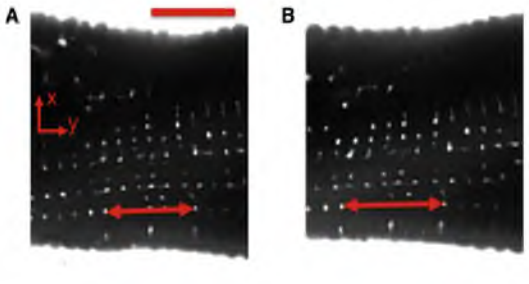

FIGURE 1 Image of myocyte segment before (*A*) and during (*B*) 15% static strain. Extracellular space and t-system exhibit fluorescent signal. Two corresponding t-tubules are marked in each image (*arrows*). Longitudinal t-tubular spacing Δ was (*A*) 1.80 and (*B*) 2.06 μm. Scale bar: 10 μm.

$\Delta_{\text{Unstrained}}$ describing the spacing after and before strain, respectively. Fractional volume of the t-system was calculated based on fluorescence ratios (9).

T-tubules were automatically segmented with the region-growing method (10). Characterization of t-tubules by principal component analysis was based on the image moments of spherical regions (10). The centers of these regions were regularly spaced (~0.2 μm) along the t-tubule longitudinal axis. Centroids of these regions $\bar{\mathbf{x}}$ were determined by first-order image moments given by

$$\bar{\mathbf{x}} = (\bar{x}_1\ \bar{x}_2\ \bar{x}_3)' = \sum_{i\in S} \mathbf{x}_i\ I(\mathbf{x}_i)\ \Big/ \sum_{i\in S} I(\mathbf{x}_i),$$

with the three-dimensional image I and the set of voxel indexes in the spherical region S. A matrix of second-order central image moments $\mathbf{M_2}$ was set up as

$$\mathbf{M}_2 = \begin{pmatrix} M_{200} & M_{110} & M_{101} \\ M_{110} & M_{020} & M_{011} \\ M_{101} & M_{011} & M_{002} \end{pmatrix},$$

with the moments

$$M_{pqr} = \sum_{i\in S} (x_{i,1} - \bar{x}_1)^p (x_{i,2} - \bar{x}_2)^q (x_{i,3} - \bar{x}_3)^r I(\mathbf{x}_i).$$

Eigenvalues, λ_1, λ_2, and λ_3, and eigenvectors, $\mathbf{e}_1$, $\mathbf{e}_2$, and $\mathbf{e}_3$, of $\mathbf{M_2}$ were calculated by singular value decomposition. Several measures served for characterization of t-tubule cross-sections: ellipticity and orientation. Ellipticity ε of tubules was defined as

$$\varepsilon = 1 - \sqrt{\lambda_3/\lambda_2}.$$

With this measure, a decrease of ellipticity corresponds to more circular cross-sections. The orientation α of the minor eigenvector $\mathbf{e_3}$, i.e., the minor axis of the t-tubule cross-section, versus the myocyte long axis $\mathbf{m}_1$, was calculated by

$$\alpha = \arctan((\mathbf{e}_3 \times \mathbf{m}_1)/(\mathbf{e}_3 \cdot \mathbf{m}_1)).$$

Only t-tubules of simple topology were used for further analysis. Mouth and end regions of the t-tubules were excluded from analysis to avoid problems with detection of these regions and image blurring.

Analysis of a t-tubule (Fig. 2) revealed that it had a length of 2.3 μm. The cross-sectional area shows a maximum at its mouth and a constriction at 0.8 μm (Fig. 2 *B*). Ellipticity ranged between 0.07 and 0.23, indicating a slight flattening of the cross sections (Fig. 2 *C*). Orientation ranged between 1 and 32° (Fig. 2 *D*).

A statistical analysis of 28 cells from 14 animals is presented in Fig. 3 and Table 1. T-tubules (n =1048) and their cross sections (n = 10,328) were grouped according to the strain of cells, i.e., control (before strain), 5% strain (2.5–7.5%), and 15% strain (12.5–17.5%). At 15% strain, mean t-tubule length and volume decreased by 10.3% and 12.7%, respectively. The fractional volume of the t-system decreased by 16.5%. The mean orientation angle of the minor eigenvector increased with increasing strain.

Our study demonstrates that cellular strain alters the shape and volume of the t-system in myocytes. The measured decrease of volume is associated with a decrease of t-tubule length. This finding contrasts with results from a previous study on the t-system from toad skeletal muscle

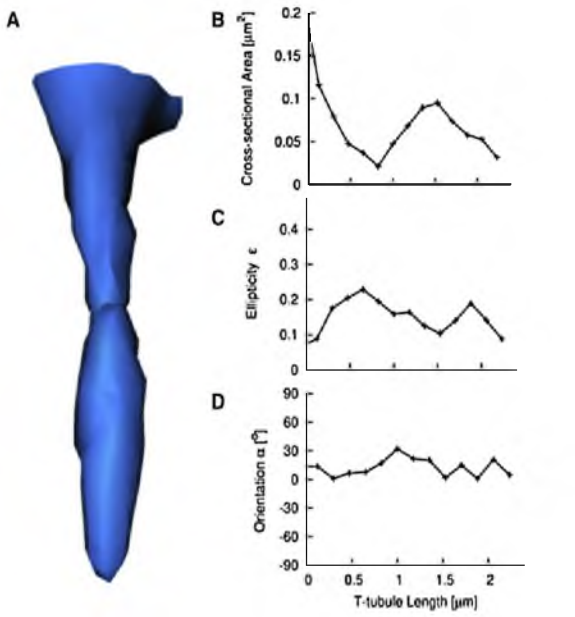

FIGURE 2 Reconstruction and analysis of t-tubule from rabbit myocyte. (*A*) Three-dimensional reconstruction of t-tubule at rest with simple topology. (*B*) Cross-sectional area, (*C*) ellipticity ε, and (*D*) orientation α were determined along the length of the t-tubule. An orientation α equal to zero denotes that the minor axis of the t-tubule cross-section is parallel to the myocyte long axis.

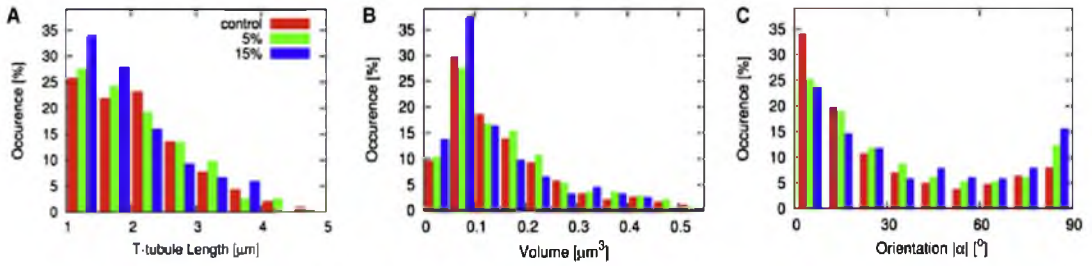

FIGURE 3 Statistical analysis. Histograms of (*A*) t-tubule length, (*B*) volume, and (*C*) orientation of cross sections are presented for control cells and cells at 5% and 15% strain. Strain was associated with an increase of short t-tubules and small volume. Cross sections of t-tubules of strained cells tended toward having minor axes perpendicular to the myocyte long axis.

TABLE 1 Statistical analysis of t-tubules presented as mean ± standard deviation

Feature	Controls	5%	15%
Length [μm]	2.12 ± 0.84	2.07 ± 0.84	1.90 ± 0.75*
Volume [μm^3]	0.16 ± 0.12	0.17 ± 0.12	0.14 ± 0.11*
Fractional volume [%]	4.82 ± 1.33	4.41 ± 1.00	4.01 ± 0.87*
Ellipticity ε	0.20 ± 0.11	0.20 ± 0.11	0.19 ± 0.10*
Orientation $\|\alpha\|$ [°]	28.7 ± 27.4	34.2 ± 28.6*	38.7 ± 30.0*

*$p < 0.05$ versus control.

fibers. Based on intensity analysis of two-dimensional confocal micrographs, it has been observed that sarcomere length, which varied in the range from 1.93 to 3.30 μm, did not affect the steady-state fractional volume (11).

Our data suggest that geometrical changes of the t-system begin at small cellular strains (5%). Geometrical changes of t-tubules are associated with changes of the stress distribution on the sarcolemma, which has been suggested as a mechanism for gating of stretch-activated ion channels (7). Further implications of our finding are related to a possible mechanism for pumping fluid into and out of the t-system. Our data on volume changes indicate that high strain (15%) along the cell long axis causes flux of fluid out of the t-system into the interstitial space.

Limitations of our imaging approach are discussed in our previous publication (2) and the Supporting Material. This study focused on the rabbit t-system. Comparative studies are needed in other species to generalize our findings.

SUPPORTING MATERIAL

Three figures and additional materials and methods are available at http://www.biophysj.org/biophysj/supplemental/S0006-3495(11)00404-8.

ACKNOWLEDGMENTS

We thank Dr. Kenneth Spitzer for useful discussions and his help in the presented studies.

This study was supported by the Richard A. and Nora Eccles Fund for Cardiovascular Research and awards from the Nora Eccles Treadwell Foundation.

REFERENCES and FOOTNOTES

1. Fawcett, D. W., and N. S. McNutt. 1969. The ultrastructure of the cat myocardium. I. Ventricular papillary muscle. *J. Cell Biol.* 42:1–45.
2. Savio-Galimberti, E., J. Frank, …, F. B. Sachse. 2008. Novel features of the rabbit transverse tubular system revealed by quantitative analysis of three-dimensional reconstructions from confocal images. *Biophys. J.* 95:2053–2062.
3. Balijepalli, R. C., A. J. Lokuta, …, T. J. Kamp. 2003. Depletion of T-tubules and specific subcellular changes in sarcolemmal proteins in tachycardia-induced heart failure. *Cardiovasc. Res.* 59:67–77.
4. Wei, S., A. Guo, …, L. S. Song. 2010. T-tubule remodeling during transition from hypertrophy to heart failure. *Circ. Res.* 107:520–531.
5. Louch, W. E., V. Bito, …, K. R. Sipido. 2004. Reduced synchrony of Ca^{2+} release with loss of T-tubules—a comparison to Ca^{2+} release in human failing cardiomyocytes. *Cardiovasc. Res.* 62:63–73.
6. Kohl, P., P. J. Cooper, and H. Holloway. 2003. Effects of acute ventricular volume manipulation on in situ cardiomyocyte cell membrane configuration. *Prog. Biophys. Mol. Biol.* 82:221–227.
7. Dyachenko, V., B. Husse, …, G. Isenberg. 2009. Mechanical deformation of ventricular myocytes modulates both TRPC6 and Kir2.3 channels. *Cell Calcium.* 45:38–54.
8. Savio, E., J. I. Goldhaber, …, F. B. Sachse. 2007. A framework for analyzing confocal images of transversal tubules in cardiomyocytes. *Lect. Notes Comput. Sci.* 4466:110–119.
9. Soeller, C., and M. B. Cannell. 1999. Examination of the transverse tubular system in living cardiac rat myocytes by 2-photon microscopy and digital image-processing techniques. *Circ. Res.* 84:266–275.
10. Gonzalez, R. C., and R. E. Woods. 1992. Digital Image Processing. Addison-Wesley, Reading, MA.
11. Launikonis, B. S., and D. G. Stephenson. 2002. Tubular system volume changes in twitch fibers from toad and rat skeletal muscle assessed by confocal microscopy. *J. Physiol.* 538:607–618.

Supplementary Information

Myocyte Preparation

The study was approved by the Institutional Animal Care and Use Committee, University of Utah. New Zealand white rabbits (~1.5 kg) were anesthetized and anti-coagulated with an intravenous administration of pentobarbital (25 mg/ml) and heparin (2500 USP units/kg). The hearts were quickly excised and placed in a cold (4 °C) zero calcium isolation solution before cannulating the aorta. The heart was reverse perfused with zero calcium isolation solution, at 30 mL/min for 7 min. During this time the blood was washed out of the atria and the ventricles. The perfusate was then changed to an enzyme solution. The enzyme solution was perfused through the heart, and recirculated for 9.5 min, before changing the perfusate to a washout solution for 5 min. After washout, the heart was minced in 50 mL of washout solution and gently shaken for 10 min before filtering off the tissue debris. $CaCl_2$ was added to the washout solution containing the dissociated myocytes, incrementally increasing the calcium concentration every 6 min from 0.05 mM until it was 0.1 or 1 mM. Myocytes were left in that solution at room temperature until used.

Solutions

The zero calcium isolation solution was composed of (in mM): 92 NaCl, 4.4 KCl, 5 $MgCl_2$, 1 $Na_2H_2PO_4$, 24 HEPES, 11 glucose, 20 taurin, 5.7 creatine, 5.0 sodium pyruvate, 12.5 NaOH. The washout solution consisted of the zero calcium isolation solution with an additional 0.05 mM $CaCl_2$. The enzyme solution consisted of the washout solution with 0.2 mg/mL Collagenase P (Roche, Mannheim, Germany) and 0.06 mg/mL protease Type XIV (Sigma, St. Louis, MO, USA).

Glass Microtools

Rupture patch electrodes were pulled using borosilicate glass capillary tubing (Schott 8250, A-M Systems Inc., Sequim, WA) and fire polished until sealed. Strain manipulators were formed by positioning the tip over a platinum-iridium heating element (~0.1 mm in diameter), which applied heat to bend the tip. The angle between the tip of the strain manipulator and the shaft were between 100-110° (Supp Fig. 2). Before use, the strain manipulators were placed in a solution of laminin (BD Biosciences, Bedford, MA) for 10 min in order to improve the adhesion

between the manipulators and the cells. The solution of laminin was made by diluting 20 μL of laminin in 100 μL of solution containing 1 mM $CaCl_2$. When adhesive strength between the manipulators and the cell was small, either an extra coat of laminin was added to retain adhesive strength or new strain manipulators were coated and used. The strain manipulators were positioned at the ends of the myocytes.

Imaging

All images were acquired within 6 h of isolation using a Zeiss LSM 5 Duo confocal microscope equipped with a 63x oil immersion lens (numerical aperture: 1.4). We imaged myocyte segments in a central region between the manipulators by three-dimensional scanning (x-, y- and z-resolution: 0.1, 0.1 and 0.2 μm) at rest and with varying strain. The x-, y- and z-dimension of the stacks were typically 32, 25, and 15 μm, respectively.

Image Deconvolution and Processing

All images were pre-processed in a similar way as described previously (1, 2). In short, the iterative Richardson-Lucy algorithm was applied with point spread functions (PSFs) extracted from images of fluorescent beads 100 nm in diameter (Molecular Probes, Eugene, OR; excitation wavelength 505 nm, emission wavelength 515 nm) residing in the first 10 μm above the cover slip. Ten images of isolated beads were averaged to determine the PSF.

Mask images of the myocytes and their t-system were generated from the dextran-fluor images by region-growing techniques and morphological operators (3). Further image processing and visualization were restricted to the mask image. Sarcomere length in image regions was determined by Fourier analysis of image stacks (Fig. 1). Longitudinal spacing Δ of the t-system was determined by maxima in Fourier spectra.

T-System Visualization and Analysis

The t-system was reconstructed using 3D visualization methods. Isosurface triangular meshes were generated with a modified marching cube algorithm (4). The meshes were visualized using custom software based on OpenGL (5) and Open Inventor (6). Exemplary visualizations are presented in Fig. 2A and Supp Fig. 3.

T-tubules were segmented in the deconvolved image stack with the region growing technique (3). First, the stacks were subdivided into cubes with a volume of ~1 μm^3. Points of maximal intensity were detected in the cubes and used as seed points for region growing. Afterwards,

region growing was performed in a six-neighborhood and with a global threshold value, which was determined by histogram analysis of intensity distributions in image stacks. Only t-tubules in the first 10 μm above the cover slip, having a length >1 μm, and non-furcated, were selected for further analysis. The analysis of the segmented t-tubules revealed their length and volume.

All analyses were implemented in Matlab (R2010b, Mathworks, Natick, MA). For each t-tubule, a centerline was fit using a least-squares method, and orthogonal cross sections were extracted. Principal component analysis of the cross-sections yielded eigenvectors $\mathbf{e}_1$, $\mathbf{e}_2$, and $\mathbf{e}_3$ associated with eigenvalues λ_1, λ_2, and λ_3 (3). The eigenvalues were used as described in the main document of this publication.

Statistical Analysis

Statistical significance was determined using an unpaired two-tailed t-test ($p<0.05$).

Limitations

Limitations of confocal microscopic imaging have been discussed in detail (7, 8). Several limitations of our experimental preparation and conditions constrain our conclusions. In particular, the static conditions of our cells are different to the dynamic environment of cells in a beating heart. Furthermore, in this study we did not analyze activated cells or cells in a strain range corresponding to cellular contraction. We did not attempt to measure strain-modulated volume changes along the t-tubule and thus cannot draw conclusions on the details of fluid exchange along t-tubules into the depth of the myocyte. Our analysis included only transverse components of simple topology and neglected longitudinal and topologically more complex components of the t-system. While transverse components of simple topology are common in the t-system of ventricular cells from rabbit, the analysis of topologically more complex t-system in other species, e.g. the network of tubules in rat, would need different approaches. Our study did not reveal the mechanisms of strain transmission from cellular level to t-system. We speculate that components of the cytoskeleton and anchor proteins are the major contributors to strain transmission.

References

1. Savio-Galimberti, E., J. I. Goldhaber, J. H. B. Bridge, and F. B. Sachse. 2007. A framework for analyzing confocal images of transversal tubules in cardiomyocytes. In Lecture notes in computer science. Springer, Berlin. 110-119.
2. Sachse, F. B., E. Savio-Galimberti, J. I. Goldhaber, and J. H. Bridge. 2008. Sub-micrometer anatomical models of the sarcolemma of cardiac myocytes based on confocal imaging. Pac Symp Biocomput:390-401.
3. Gonzalez, R. C., and R. E. Woods. 1992. Digital Image Processing. Addison-Wesley, Reading, MA.
4. Heiden, W., T. Goetze, and J. Brickmann. 1991. 'Marching-Cube'-Algorithmen zur schnellen Generierung von Isoflächen auf der Basis dreidimensionaler Datenfelder. In Visualisierung von Volumendaten. M. Frühauf, and M. Göbel, editors. Springer, Berlin, Heidelberg, New York. 112-117.
5. Shreiner, D., M. Woo, J. Neider, and T. Davis. 2003. OpenGL programming guide: The official guide to learning OpenGL. Addison-Wesley, Reading, MA.
6. Wernecke, J. 1994. The inventor mentor: Programming object-oriented 3d graphics with Open Inventor. Addison-Wesley, Reading, MA.
7. Savio-Galimberti, E., J. Frank, M. Inoue, J. I. Goldhaber, M. B. Cannell, J. H. Bridge, and F. B. Sachse. 2008. Novel features of the rabbit transverse tubular system revealed by quantitative analysis of three-dimensional reconstructions from confocal images. Biophys J 95:2053-2062.
8. Bolte, S., and F. P. Cordelieres. 2006. A guided tour into subcellular colocalization analysis in light microscopy. J Microsc 224:213-232.

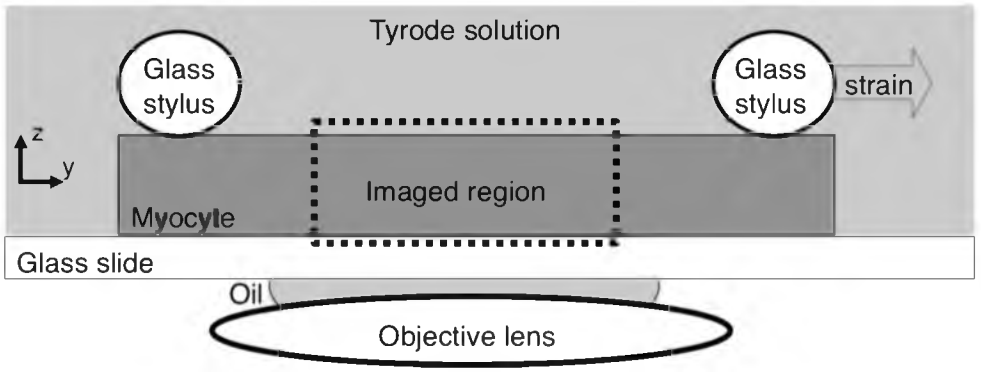

Supp Fig. 1: Setup for imaging and applying strain to a myocyte. The myocytes are held between two laminin coated glass styli and the glass slide. Strain is applied by translation of a glass stylus using a motorized micro-manipulator.

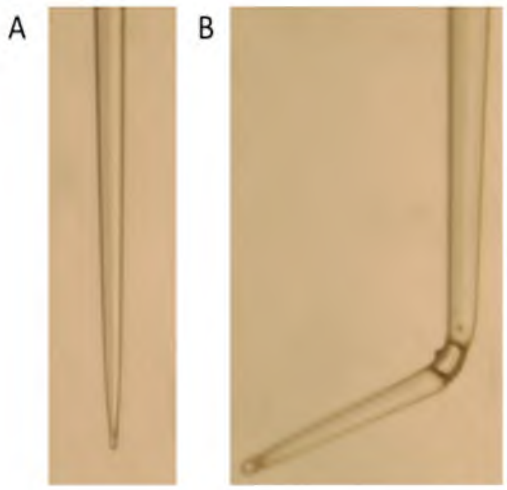

Supp Fig. 2: Glass microtool for applying strain. (A) A micropipette with an outer diameter of ~15 μm was sealed. (B) Afterwards it was bent by applying heat, forging a strain manipulator. The manipulator is attached to micro-manipulator and subsequently coated with laminin.

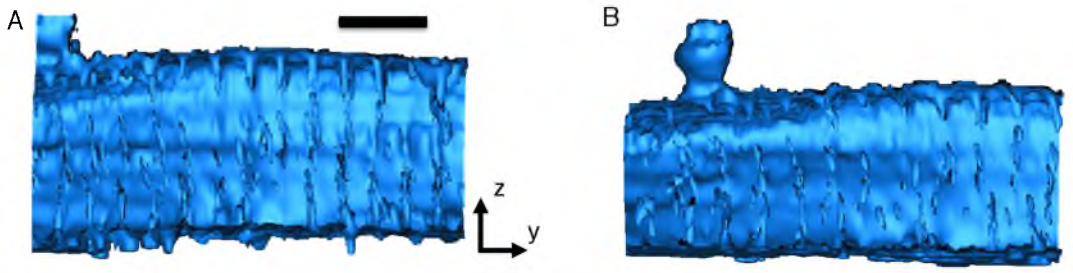

Supp Fig. 3: Reconstruction of t-system in a myocyte segment before (A) and while applying 15% strain (B). Scale bar: 5 µm.

4. GEOMETRIC CHANGES IN RABBIT CARDIAC TRANSVERSE TUBULAR SYSTEM DUE TO CONTRACTION AND MECHANICAL DEFORMATION

Introduction

Many types of mammalian cardiac myocytes exhibit a transverse tubular system (t-system), which consists of sarcolemmal invaginations[1]. Despite the name, the t-system has been shown to comprise variable degrees of longitudinal components depending on species[2-5]. For example, in rat cardiomyocytes, the t-system forms a highly connected network with transversal and longitudinal components[2, 4]. In rabbit, on the other hand, the t-system has more transversally oriented and unconnected tubules, looking like fingers poking into the cell[3, 5]. The existence of the t-system is also species dependent, being present in mammalian cardiac myocytes, while being absent in avian, reptile, and amphibian cardiac tissue[6].

The t-system plays an important role in excitation contraction coupling. Calcium is the major signaling molecule in excitation contraction coupling, and many proteins involved in calcium signaling are closely associated with the t-system[4, 7, 8]. Another role of the t-system is in electrical signaling. The lumen of t-tubules connects directly to the extracellular space and this connection allows electrical signals to enter deep into the cell at a much faster velocity than diffusion of ions from the outer sarcolemma through the intracellular space[6, 9]. Thus, the t-system is crucial for coordinated contraction within the

myocyte. Alterations of t-system density have been shown to occur in heart failure and exercise[10-12] and to affect excitation contraction coupling[10, 13].

Mechanical and structural properties of the t-system are still not well characterized. For instance, mechanisms of strain transfer from cellular level to the t-system are not understood. Various cytoskeletal proteins are adjacent to the t-system, which suggests mechanisms that allow for strain transfer to the t-tubules[14, 15]. This transfer of strain is important for mechanical signaling to ion channels, for instance, to nonselective stretch activated ion channels residing only in the t-system[16].

The association of various ion channels with the membrane of t-tubules is not the sole contribution of the t-system to the electrophysiology of the heart. Depending on species and cell type, the t-system is an important contributor to the myocyte surface-to-volume ratio and the membrane capacitance[10, 17, 18]. It has been hypothesized that membrane capacitance increases as strain is applied to cardiac tissue[19, 20]. Any change of membrane capacitance can be expected to strongly affect conduction velocity in tissue[21]. However, a direct measurement of strain-modulated capacitance of the sarcolemma and the t-system has not been carried out.

Recently, we demonstrated that strain at the cellular level is transmitted to the t-system, reducing the length and volume of tubules and altering their cross-sectional shape[5]. Our data suggest that a cellular strain of as little as 5% affects the shape of transverse tubules. Our study supports a prior hypothesis that strain can cause fluid exchange between the t-system and extracellular space.

Here, we extended these studies to gain insights into the effects of cellular contraction on the t-system. We hypothesize that cellular contraction affects the t-system geometry,

in particular, that length and volume of t-tubules increase in contracted cells. We tested this hypothesis using our previously developed confocal imaging approach on living and fixed myocytes as well as electron microscopy (EM) on fixed cardiac tissues. In this study, we also intend to shed light on functional consequences of strain-modulated t-tubular geometry using whole cell voltage clamping approaches. Finally, we studied the relationship between t-tubules and a cytoskeletal protein, i.e., actinin, to propose a hypothesis on strain-modulation of t-tubule geometry via the cytoskeleton.

Methods

Solutions

The zero calcium isolation solution was composed of (in mM): 92 NaCl, 4.4 KCl, 5 $MgCl_2$, 1 $Na_2H_2PO_4$, 24 HEPES, 11 glucose, 20 taurin, 5.7 creatine, 5.0 sodium pyruvate, 12.5 NaOH. The enzyme solution consisted of the zero calcium isolation solution with 0.2 mg/mL Collagenase P (Roche, Mannheim, Germany), 0.06 mg/mL protease Type XIV (Sigma, St. Louis, MO, USA), and a final concentration of 0.05 mM $CaCl_2$. The washout solution consisted of the zero calcium isolation solution with 0.05 mM calcium. The modified Tyrode's solution was composed of: 126 NaCl, 4.4 KCl, 5 $MgCl_2$, 24 HEPES, 11 glucose, 12.5 NaOH, and 1.0 $CaCl_2$. The zero sodium solution was similar to the modified Tyrode's solution except, NaCl was replaced (mole for mole) with N-methyl-D-glucamine, $CaCl_2$ was 2.0 mM, and the solution was titrated to pH 7.4 using HCl. The tonic contraction solution consisted of 10 mM caffeine added to the zero sodium solution. The pipette solution was composed of 110 KCl, 5 NaCl, 5 MgATP, 5 Phosphocreatine (dipotassium salt), 1 NaGTP, 10 HEPES, and was titrated with 1 N KOH to pH 7.1–7.2.

Isolated Myocyte Preparation

The methods for isolating cardiac myocytes from rabbit ventricular myocytes were published previously[5]. In short, New Zealand white rabbits (1.7 – 2.0 kg) were anesthetized and anticoagulated with an intravenous administration of pentobarbital (25 mg/ml) and heparin (2500 USP units/kg). The hearts were quickly excised and cannulated for Langendorff perfusion. The hearts were reverse perfused with zero calcium isolation solution, at 40 mL/min for 5 min, followed by 12 min of perfusion with enzyme solution, and then 5 min of perfusion with washout solution. After washout, the hearts were minced in 50 mL of washout solution and gently shaken for 10 min before filtering off the tissue debris. Calcium was added to the washout solution containing the dissociated myocytes, incrementally increasing the calcium concentration to 1 mM.

Contracted Myocytes Preparation

Isolated myocytes were placed in a flow through chamber coated with laminin. After the cells settled, dead cells and debris were washed away with the modified Tyrode's solution. This was followed by a change to zero sodium solution. After a few minutes of high flow with zero sodium solution, the solution was changed to the tonic contraction solution. After ensuring the tonic contraction solution had washed in, the flow was stopped.

In Vitro Labeling, Imaging and Image Processing

After stopping the flow of solutions over the myocytes, a fluorescent dye, conjugated to a membrane impermeable dextran molecule (Alexa 488, Invitrogen, Carlsbad, CA), was added to the solution. Imaging was done on a Zeiss LSM 5 Duo microscope, using

an oil immersion 63x objective with a numerical aperture of 1.4. Raw images of segments from a contracted myocyte are shown in Fig. 4.1. Image stacks were preprocessed, segmented, and analyzed as described previously[5]. In short, an iterative Richardson-Lucy deconvolution algorithm was applied to the images with a point spread function extracted from images of fluorescent beads 100 nm in diameter (Molecular Probes, Eugene, OR; excitation wavelength 505, emission wave length 515 nm) within the first 10 µm above the cover slip. T-tubules were segmented in deconvolved images. Only t-tubules in the first 10 µm above the cover slip, having a length >1 µm, and nonfurcated, were selected

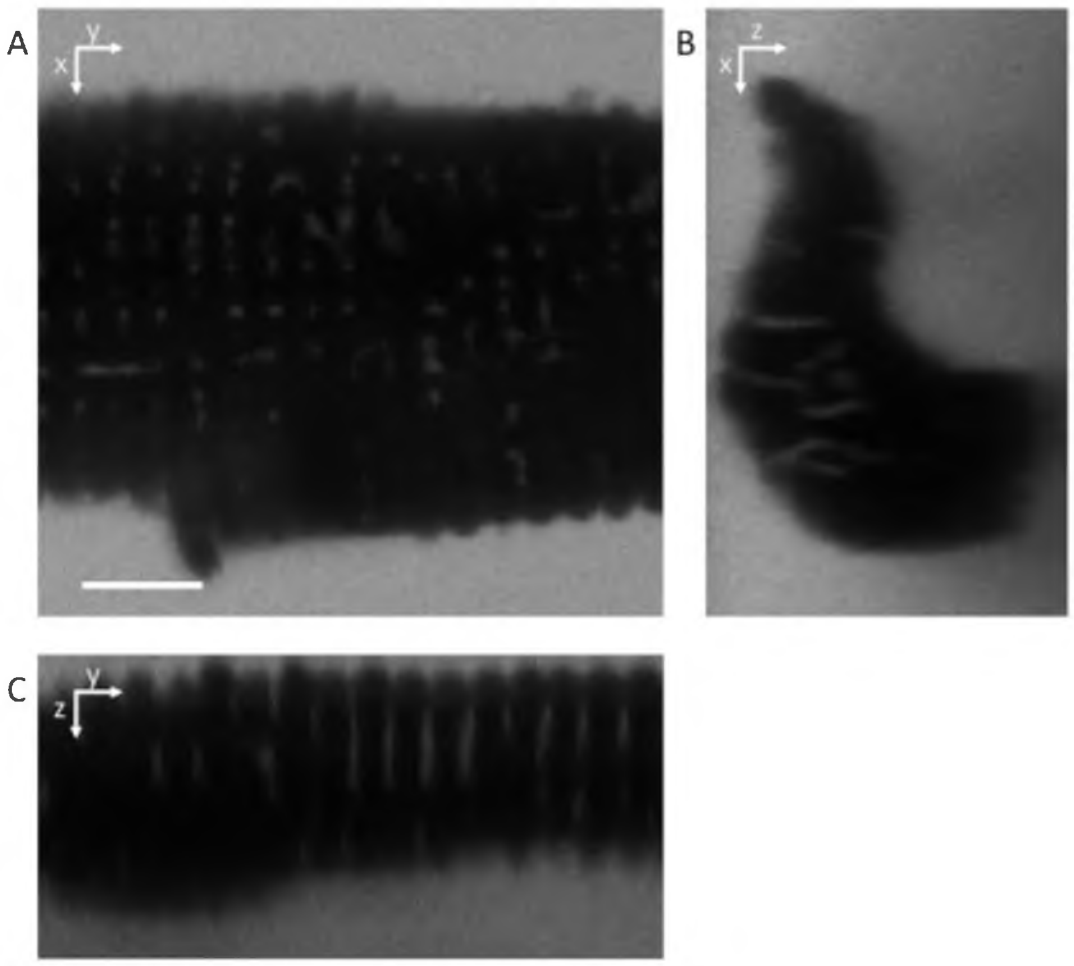

Figure 4.1: Central cross sections from image stacks of segments from contracted myocyte. Top view (A), end view (B), and side view (C). Scale bar: 5 µm.

for further analysis. For each t-tubule, a centerline was fit using a least-squares method, and orthogonal cross sections were extracted. Principal component analysis of the cross-sections yielded eigenvectors $\mathbf{e_1}$, $\mathbf{e_2}$, and $\mathbf{e_3}$ associated with eigenvalues λ_1, λ_2, and λ_3 [22]. Ellipticity, ε, of a t-tubule cross-section was defined as:

$$\varepsilon = 1 - \sqrt{\lambda_3 / \lambda_2}$$

The orientation angle of the t-tubule minor axis, α, was zero when parallel with the myocyte long axis. Fractional t-tubule volume was calculated as previously described[2].

Fixation and Fluorescent Labeling

Cells were fixed in contraction using a 2% paraformaldehyde solution and were labeled with wheat germ agglutinin (WGA) conjugated to Alexa 555 (Invitrogen, Carlsbad, CA). After treatment with 0.05% Triton-X-100 and washing, a blocking solution containing 10% normal goat serum was applied. Further labeling was done using primary antibodies (mouse) for α-actinin (Sigma-Aldrich, St. Louis, MO), which is a protein associated with the Z-disks. The secondary antibody applied was goat anti mouse conjugated to Alexa 488 (Invitrogen, Carlsbad, CA).

Electron Microscopic Imaging and Analyses

Preparations of cardiac ventricular tissue from New Zealand white rabbits were prepared for EM imaging as described previously[19]. In short, isolated hearts were quickly mounted to a Langendorff perfusion system for retrograde perfusion at 37° C. After washout, one of two different perfusates was used, one to induce contraction, or an alternative to induce cardioplegia. Three different states of the heart were produced:

resting, strained (via fluid filled balloon), and contraction. Afterwards the heart was fixed and the tissue was prepared for EM imaging.

Images had a dimension of 2896 x 3728 pixels. The image resolution ranged between 400-714 pixels/μm. In these images, we measured the mean sarcomere length (SL) and the mean length of the A-bands. The ratio of A-band length to SL (A-Z ratio) was determined as an indicator of strain, independent of the angle of the slice with regards to the sarcolemma[23]. The relationship between A-Z ratio and SL is shown in Fig. 4.2. A linear fit was performed to describe the A-Z ratio as a function of SL:

$$A\text{-}Z\ ratio = -0.34\ SL + 1.43$$

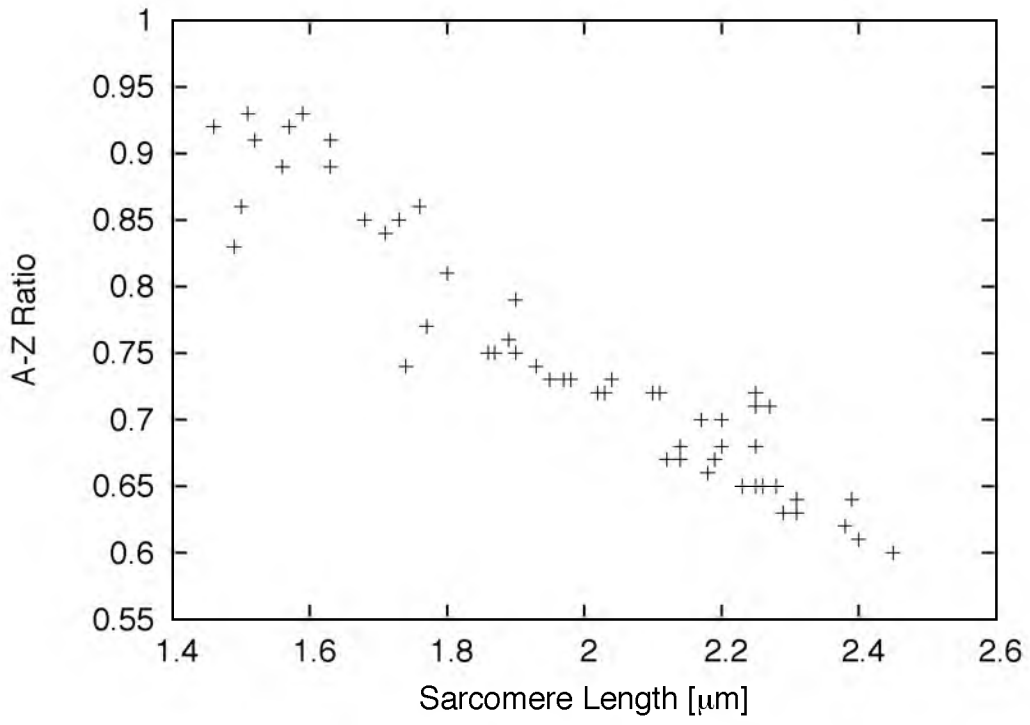

Figure 4.2: Relationship between A-Z ratio and SL. A linear fit (y=ax+b) using the least squares method yielded slope of a = -0.34 and a constant of b = 1.43. The fit line had an R^2 value of 0.89.

with R^2=0.89. T-tubule cross-sections were segmented using the Matlab function roipoly in order to calculate their area, orientation of the minor axis, and ellipticity. Two-dimensional principle component analysis was applied to determine the ellipticity and orientation of the segmented t-tubule cross-sections. Fourier transform was used to determine the orientation of the sarcomeres in each slice. The orientation angles of t-tubule cross-sections were determined relative to the sarcomere orientation. Changes in angle were specified as differences between the sarcomere and t-tubule minor axis orientation.

Voltage Clamping of Strained Cells

The membrane capacitance C_m was calculated based on an approximation of the cell membrane as in the electrical RC-diagram (Fig. 4.3). The measured values were calculated using the equations derived from the schematic as follows:

$$R_a = V_c / i_{\min}$$

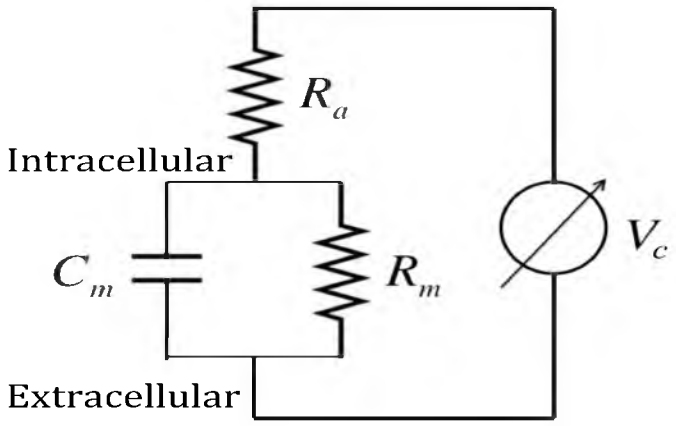

Figure 4.3: Electrical schematic representing the components of the voltage clamp set-up with voltage clamp input V_c, access resistance R_a, membrane resistance R_m, and membrane capacitance C_m.

$$i_{SS} = V_C / (R_m + R_a)$$

$$R_p = \frac{R_a \times R_m}{R_a + R_m}$$

$$\tau = R_p C_m$$

with the access resistance R_a, the clamped voltage V_c, the minimum of the current response i_{min}, the steady state current i_{SS}, the membrane resistance R_m, the time constant of the current response τ, and the membrane capacitance C_m. The current response to the voltage clamp step was fit with a mono-exponential linear function[24]. Measurements from each cell were normalized to the values recorded during control.

The experiments were performed on resting and strained rabbit ventricular myocytes held in a glass-bottom, flow-through cell chamber at 35°C. Glass micro-pipettes with bent tips, as described previously[5], were used in order to apply strain. With the patch electrode positioned near the center of the cell it was possible to apply approximately 10% strain. With the electrode positioned at the end of the cell we were able to strain it beyond 10% without losing the seal around the membrane. Cells were voltage clamped (ruptured patch) via a suction pipette. Before and during application of strain, current responses were measured while applying 5 mV-hyperpolarizing steps (Fig. 4.4), the duration being 200 ms from a holding potential at the resting membrane voltage. The electrical stepping protocol was applied as control (before pressing the glass tools on the cell), after pressing on the cell, and after applying strain to the cell. Multiple measurements were taken during

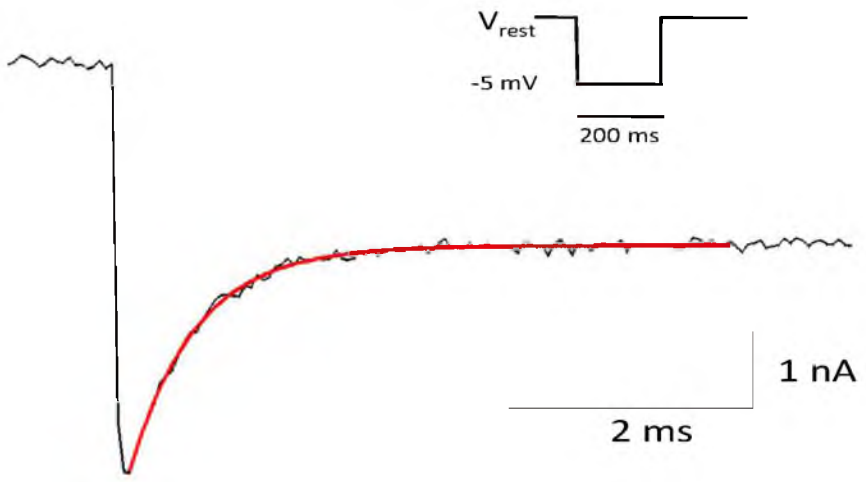

Figure 4.4: Current response to voltage clamp protocol applied to a ventricular myocyte. The mono-exponential fit to the current response is shown in red. Inset shows the voltage protocol applied to the myocyte. V_{rest} is set at the resting membrane voltage identified by absence of membrane current.

control, pressing, and strain. The mean of those measurements per cell was determined for each cell. Strains considered for analysis were at minimum 10% increase from control. The average applied strain was 11.4±2.8%. Data from cells that slipped below 10% strain at any point during measurement were excluded from analysis.

Analyses and Statistics

All analyses were implemented in Matlab (R2010b, Mathworks, Natick, MA). Data are presented as mean±standard deviation. Statistical significance was evaluated using a student's t-test. A value of $p<0.05$ was considered significant.

Results

Confocal Imaging of Living Cardiomyocytes

Three-dimensional image stacks were acquired from 101 cells from 21 animals. Examples for images of cells in rest, contraction and strain are shown in Fig. 4.5. In these analyses, we used data from resting and strained cells that we previously reported[5] to complement the data from contracted cells.

Only cells with high contrast between the t-system and the intracellular space and without significant numbers of vacuoles were analyzed. Statistical analyses of t-tubules are presented in Fig. 4.6 and Table 4.1. The number of t-tubules and cross-sections analyzed was 1,961 and 19,700, respectively. T-tubules were categorized according to the type and level of strain applied, i.e., control (0±4%), 8% strain (8±4%), 16% strain (16±4%), 8% contraction (-8±4%), or 16% contraction (-16±4%). During 16% contraction, mean t-tubule length and volume increased by 13.9 and 16.6%, respectively. Changes at 8% contraction were insignificant. The difference in t-tubule length and volume, when comparing 16% contracted with 16% strained cells, was statistically

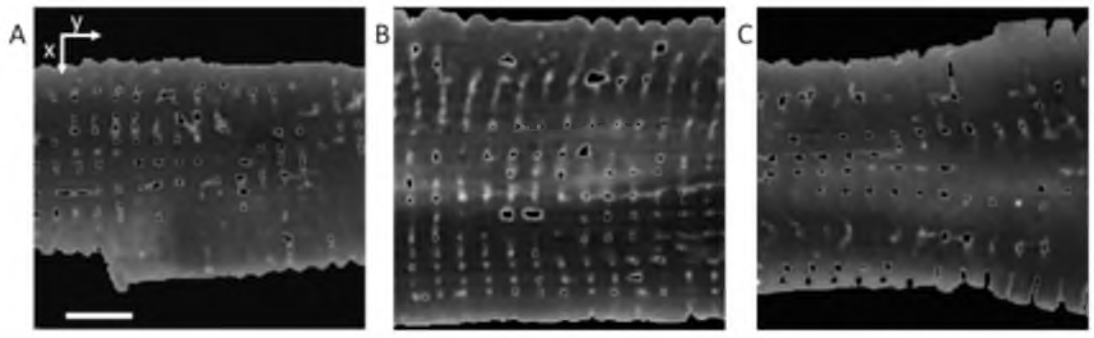

Figure 4.5: Processed images of cells in contraction (A), control (B), and strain (C). Masks were applied to each image stack to identify the cell including its t-system. The t-tubules were segmented using a region growing method. Scale bars: 5 µm.

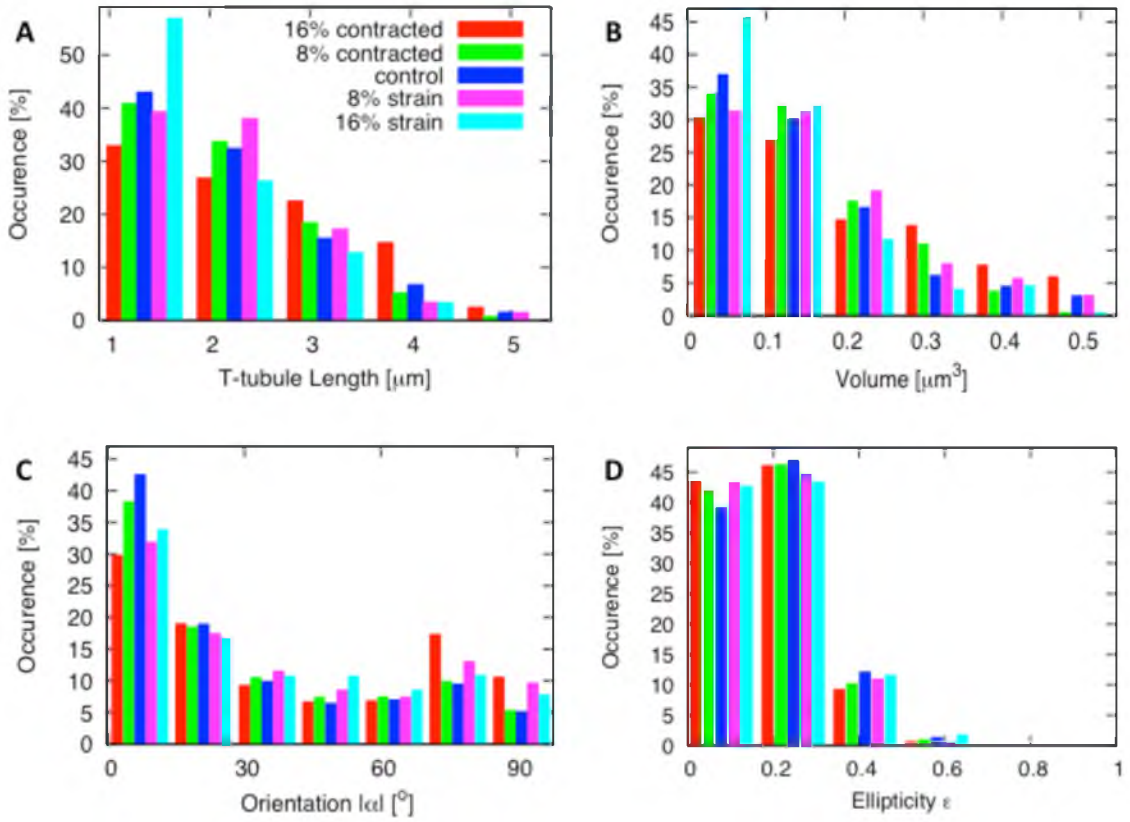

Figure 4.6: Statistical analysis of t-tubules segmented in confocal image stacks. Histograms of (A) t-tubule length, (B) volume, (C) orientation and (D) ellipticity of cross-sections are presented during contraction, control, and 16% strain. T-tubule length and volume showed an increase during contraction and a decrease during 16% strain. The orientation of t-tubule minor axis changed in both contracted and strained state, more often becoming perpendicular to the long axis of the myocyte. Sarcomere length of 1.89 μm = 0% strain.

significant. Factional t-tubule volume increased in 16% contracted cells, but remained insignificant.

The distribution of the minor axis orientation of t-tubules in control was 29.4±27.6°. During 16% contraction the distribution changed in similar manner to t-tubules in 16% strain (39.4±30.9° for 16% versus 35.3±28.9° for 16% strain); yet, the difference between 16% contraction and strain was large enough to be significant when analyzing confocal images. Ellipticity in control was 0.207±0.114. The difference in ellipticity between 16%

Table 4.1: Statistical analyses of t-tubules from confocal microscopic images of living cells.

	16% Contraction	Intermediate Contraction	Control	Intermediate Strain	16% Strain
Number of t-tubules	115	334	1021	312	170
Number of animals	3	6	17	12	11
Length [μm]	2.42± 0.98*‡	2.15±0.85	2.12±0.92	2.11±0.83	1.84± 0.72**‡
Volume [μm^3]	0.19± 0.13*‡	0.16±0.10	0.16±0.13	0.17±0.12	0.13± 0.10**‡
Fractional Volume [%]	4.92±0.79	4.61±1.06	4.76±1.13	4.66±1.57	4.15±1.00
Ellipticity ε	0.191± 0.109**†	0.199±0.106**	0.207±0.114	0.195±0.106**	0.204± 0.115†
Orientation |α|[°]	39.4± 30.9**‡	29.4±30.4	29.4±27.6	37.2± 29.9**	35.3± 28.9**‡

* Significant ($p<0.05$) vs control. ** Significant ($p<0.001$) vs control. † Significant ($p<0.01$) 16% contracted vs 16% strained. ‡ Significant ($p<0.001$) 16% contracted vs 16% strained.

contraction and strain (0.191±0.109 for 16% versus 0.204±0.115 for 16% strain) was also significant.

Confocal Imaging of Fixed Cardiomyocytes

We imaged 40 cells labeled with WGA and actinin from 5 different animals. Eight images were not processed because of low signal-to-noise ratio, drift and significant numbers of vacuoles. Raw images are presented in Fig. 4.7. The SL was measured in two

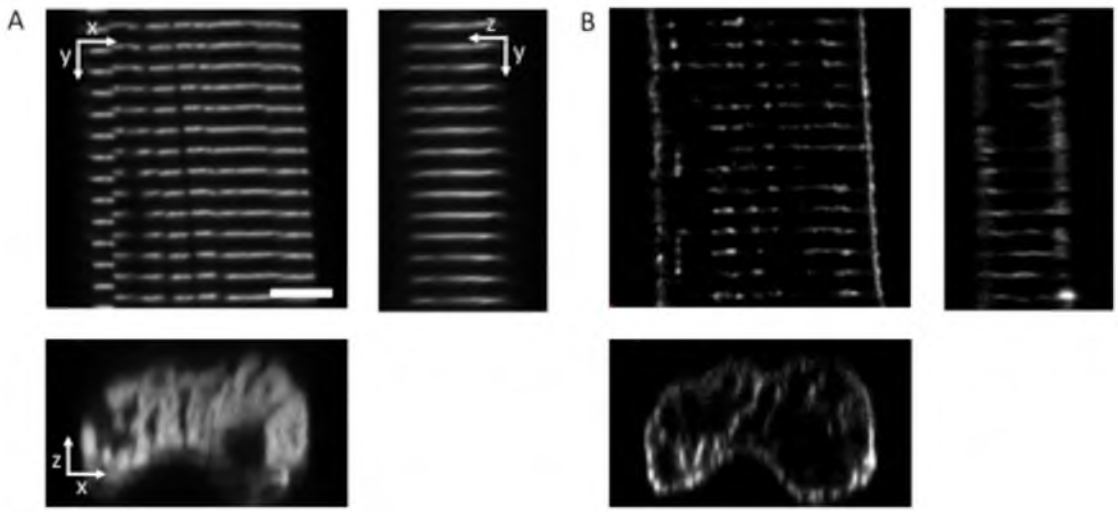

Figure 4.7: Raw sections from image stacks of segments from fixed cells labeled for actinin (A) and WGA (B). Scale bar: 5 μm.

ways, both using Fourier analysis. One method was to measure the periodicity of the labeled t-tubules, while the other method measured the periodicity of the actinin bands. The average SL of myocytes exposed to the tonic contraction protocol before being fixed (number of cells: 21, animals: 4) was 1.5804±0.0575 and 1.5833±0.1151 μm; the first being measured via actinin spacing and the second being via t-tubule spacing. The spacing of actinin distributions in control cells was 1.747±0.087 μm (number of cells: 11, Fig. 4.8), while the spacing of t-tubules was 1.745±0.114 μm.

EM Imaging of Cardiomyocytes

We analyzed 56 images and 172 t-tubules. Fig. 4.9 shows representative images from each group. All images and their t-tubule cross-sections were grouped according to the A-Z ratio associated with the corresponding ranges using SL (control 0±4%, 8±4%, and 16±4% for both contraction and strain). Changes in t-tubule ellipticity and cross-sectional area were insignificant. The orientation of the t-tubule cross-sections with respect to the

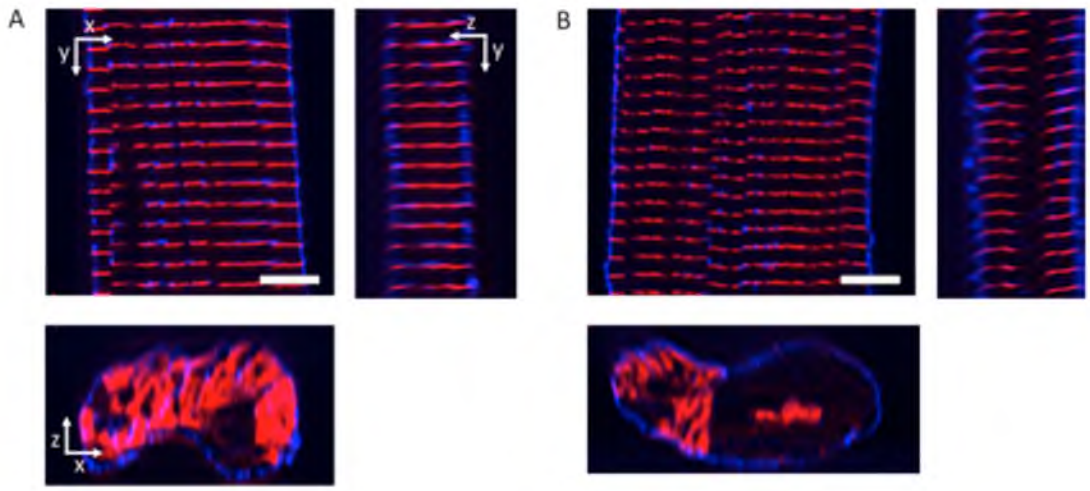

Figure 4.8: Processed sections from image stacks of segments from fixed cells in rest (A) and contraction (B). Actinin signals are shown in red. WGA signals are shown in blue. Scale bar: 5 µm.

longitudinal direction of the cell changed with strain (number of animals: 2, number of t-tubule cross-sections: 27, $p<0.05$) from 30.3±25.0° to 47.5 ± 28.6°. The mean SL in strained preparations was 2.24±0.1 µm, while the A-Z ratio was 0.671±0.036. There was a similar change in orientation of t-tubules for contracted tissue (Fig. 4.10) (SL being 1.71±0.15 µm and A-Z ratio being 0.903±0.024) to 43.6±27.5° (number of animals: 2, number of t-tubules: 82, $p<0.05$). The SL measured in control tissue was 1.91±0.047 µm and the A-Z ratio was 0.746±0.015 (number of animals: 2, number of t-tubule cross-sections: 19).

Electrical Measurements

We studied 13 isolated ventricular myocytes. The range of capacitances measured during control was 100-219 pF, with a mean of 131±36 pF. An exemplary set of measurement results is shown in Fig. 4.11. Changes in cellular capacitance were not

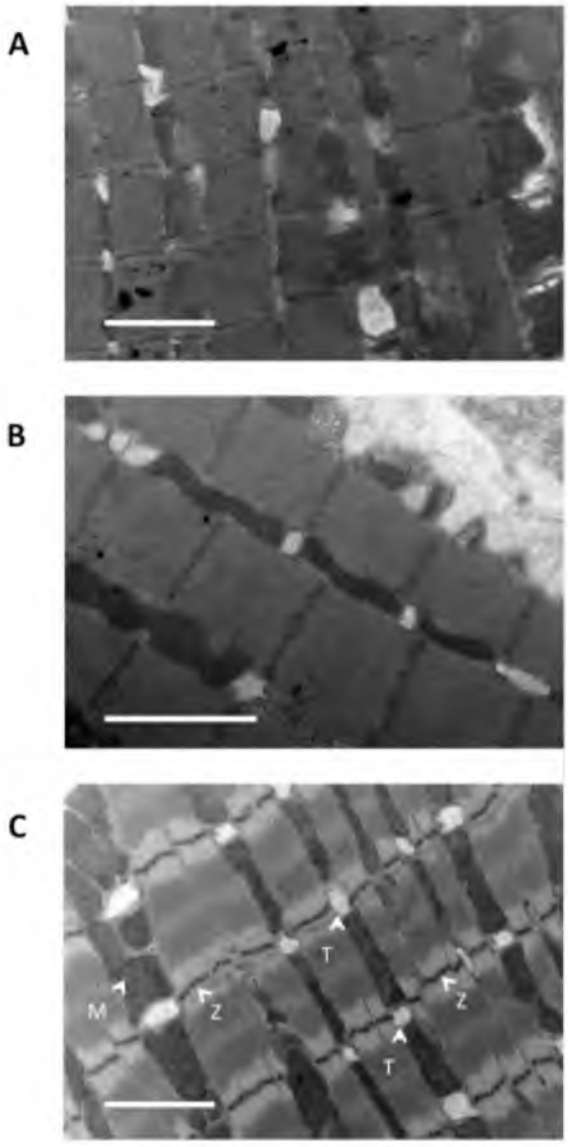

Figure 4.9: Electron micrograph images of cardiac tissue in contraction (A), control (B), and strain (C). In (C), t-tubules (T), Z-lines (Z), and mitochondria (M) are marked. Scale bars are 2 μm in length. Micrographs are courtesy of Peter Kohl and Hilary Holloway.

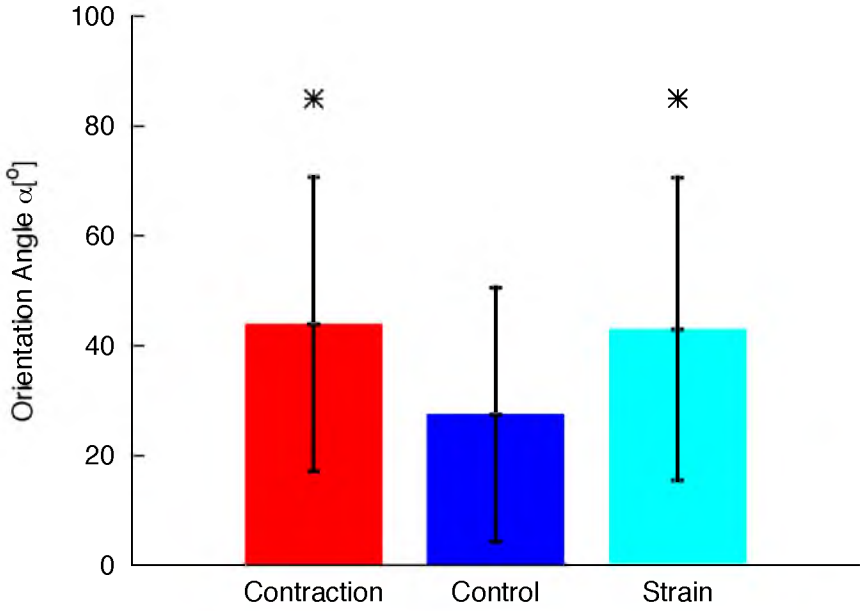

Figure 4.10: Change in angle between t-tubule minor axis and the longitudinal axis of the myocyte. Notice that angle increases in both contraction and strain ($p<0.05$). Error bars show standard deviation.

significantly affected by strain 0.99±0.04% or pressing on the cell 1.01±0.03%. Membrane resistance significantly increased by 9±7% when pressure was applied to the manipulators on the myocytes. Membrane resistance increased by 11±13% versus control, when strain was applied.

Discussion

In the presented study, we applied several imaging methods to elucidate the effects of mechanical strain on the t-system in cardiomyocytes. Fluorescent labeling, confocal imaging and image processing were used to study geometrical properties of the t-system in living myocytes in contraction, in rest, and strained. Similar methods were applied to fixed myocytes in contraction and in rest to describe the spatial relationship between t-tubules and actinin. Furthermore, electron micrographs of cardiomyocytes in contraction,

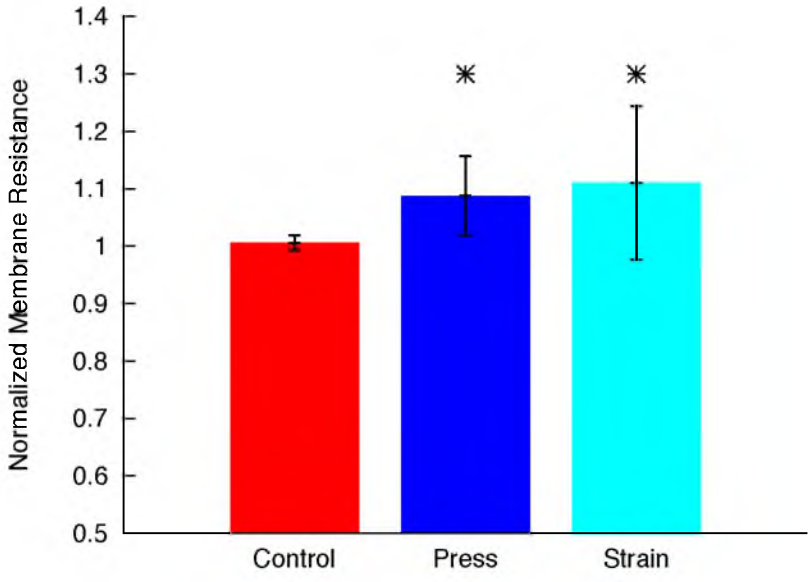

Figure 4.11: Distribution of normalized membrane resistance measurements. Membrane resistance increased as mechanical deformation was increased. Membrane resistance increased by 9±7% from control when pressure was applied to the myocytes ($p<0.001$) and 11±13% from control when strain was applied ($p<0.05$), (number of cells = 12). Error bars show standard deviation.

in rest, and strained were analyzed to study changes in orientation of the t-tubule cross-sections with respect to the actin filaments due to mechanical deformation. Finally, we measured electrical properties of myocyte membranes to investigate if strain would affect these properties.

Up until recently, little has been known regarding the cardiac t-tubule structure during the mechanically dynamic state of the cardiac cycle. A study measuring fractional volume in toad skeletal muscle at 170% strain found no change[25]. Even though the study reported measured fractional volume, the imaging protocol applied lacked sufficient imaging in three dimensions to consider the full length of t-tubules within a myocyte, which is the major source of the change in volume in our studies.

Our study revealed increased volume and length of t-system during contraction, which complements our previous findings of decreased t-tubule volume and length when myocytes are strained by 15%. We found that the change in ellipticity was the same direction when comparing the 16% strain group with the 16% contraction group and also the orientation of the t-tubule minor axis was similar for these two groups. These findings indicate that strain effects on t-tubule cross-section geometry are similar for cells in contraction and strain. It appears difficult to explain these findings with a homogeneous model of mechanical properties of the myocytes.

Fixed cells labeled with WGA and alpha-actinin showed that t-tubule movement in contraction was concordant with movement of the Z-disk. This indicates that t-tubules are anchored to Z-disks. The immunolabeling of cells exposed to the tonic contraction protocol also verifies the effectiveness of said protocol.

The analyses of EM images were partly in agreement with the analyses of the three-dimensional confocal images. During strain and contraction the orientation of the minor axis of the t-tubules changes in a similar direction. Though the changes for contracted tissue were not significant they trended towards significance having $p=0.06$. We believe that, given more image data, the change in minor axis orientation will be significant as well.

The measured t-tubule ellipticity did not significantly change in the EM images for tissue either in the strained or contracted state. There may be two reasons for an insignificant change in ellipticity in the EM images, which can be explained by stating: It is difficult to achieve electron micrograph sections that are orthogonal to the t-tubules. First, variability in the slicing angles affects the shape of the t-tubule cross-sections and

in return affect the ellipticity[23]. Second, t-tubules can be curved (see [3] for examples). In the image analysis of three-dimensional confocal microscopies, cross-sections were perpendicular to the t-tubule long axis, allowing a more robust measurement of ellipticity.

Considering the change in t-tubule length and volume with contraction and strain, we expected that the effective surface area of the sarcolemma in the lumen to change, affecting cellular capacitance[5, 19]. The electrical measurements recorded here suggest that the effective surface area of the sarcolemma remained unaffected by mechanical perturbations, including pressing on the cell and increasing strain along the longitudinal axis of the myocyte. There are three caveats to these measurements. First, although membrane capacitance appears to be independent of strain in myocytes, it remains possible that capacitance in tissue could change by way of changes in support cells and surrounding structure [20]. Second, the approach used in analyzing membrane capacitance was based on one time constant, using a monophasic exponential fit. While the fit quality was high, Fozzard described the possibility of measuring two time constants, one from the surface of the cell and another from the t-tubular lumen[26]. If the two time constants can be separated, then it may be determined that the capacitance of the t-tubules decreases, while that of the sarcolemma increases. Third, the local pressing and application of longitudinal strain is not identical to the type of strain a cell would experience in tissue. Thus, it remains possible that myocyte capacitance in tissue changes with increased strain.

The increase in membrane resistance was likely due to reduction of the conductance of inward rectifying potassium channels[27, 28]. Since the mean membrane resistance only increased by 11% when strain was applied, we presume that increased activation of non-

selective stretch activated ion channels was still smaller than the reduction of the conductance of inward rectifying potassium channels.

Limitations

We discussed limitations of the confocal imaging and analysis approach in our previous publication[5]. The method used to induce tonic contraction in living myocytes involved locking intercellular calcium within the cell by changing the perfusate to a zero sodium solution. This inhibited calcium efflux through the sodium calcium exchanger, which is the major path of calcium efflux to the extracellular space[29]. The addition of caffeine to the solution caused the ryanodine receptors to open releasing calcium stored in the sarcoplasmic reticulum, inducing contraction. However, calcium in the cytosol is not only useful in inducing contraction; it also plays a major role in the apoptotic pathway by causing calcium overload in the mitochondria[30, 31]. Thus, imaged cells that showed no t-tubules connected to the sarcolemma were considered in a state of apoptosis. A possible remedy for this problem may be to use Ru360, which blocks mitochondrial calcium uptake[32, 33].

Acknowledgements

This work was supported by the Richard A. and Nora Eccles Fund for Cardiovascular Research and awards from the Nora Eccles Treadwell Foundation.

References

1. Fawcett DW, McNutt NS. The ultrastructure of the cat myocardium. I. Ventricular papillary muscle. *J Cell Biol.* 1969;42:1-45

2. Soeller C, Cannell MB. Examination of the transverse tubular system in living cardiac rat myocytes by 2-photon microscopy and digital image-processing techniques. *Circ Res.* 1999;84:266-275

3. Savio-Galimberti E, Frank J, Inoue M, Goldhaber JI, Cannell MB, Bridge JH, Sachse FB. Novel features of the rabbit transverse tubular system revealed by quantitative analysis of three-dimensional reconstructions from confocal images. *Biophys J.* 2008;95:2053-2062

4. Asghari P, Schulson M, Scriven DR, Martens G, Moore ED. Axial tubules of rat ventricular myocytes form multiple junctions with the sarcoplasmic reticulum. *Biophys J.* 2009;96:4651-4660

5. McNary TG, Bridge JHB, Sachse FB. Strain transfer in ventricular cardiomyocytes to their transverse tubular system revealed by scanning confocal microscopy. *Biophys J.* 2011;100:L01-L03

6. Brette F, Orchard C. T-tubule function in mammalian cardiac myocytes. *Circ Res.* 2003;92:1182-1192

7. Crossman DJ, Ruygrok PR, Soeller C, Cannell MB. Changes in the organization of excitation-contraction coupling structures in failing human heart. *PLoS One.* 2011;6:e17901

8. Brette F, Sallé L, Orchard C. Quantification of calcium entry at the t-tubules and surface membrane in rat ventricular myocytes. *Biophys J.* 2006;90:381-389

9. Cordeiro JM, Spitzer KW, Giles WR, Ershler PE, Cannell MB, Bridge JH. Location of the initiation site of calcium transients and sparks in rabbit heart purkinje cells. *J Physiol.* 2001;531:301-314

10. Louch WE, Bito V, Heinzel FR, Macianskiene R, Vanhaecke J, Flameng W, Mubagwa K, Sipido KR. Reduced synchrony of Ca2+ release with loss of t-tubules a comparison to Ca2+ release in human failing cardiomyocytes. *Cardiovasc Res.* 2004;62:63-73

11. Balijepalli RC, Lokuta AJ, Maertz NA, Buck JM, Haworth RA, Valdivia HH, Kamp TJ. Depletion of t-tubules and specific subcellular changes in sarcolemmal proteins in tachycardia-induced heart failure. *Cardiovasc Res.* 2003;59:67-77

12. Kemi OJ, Hoydal MA, Macquaide N, Haram PM, Koch LG, Britton SL, Ellingsen O, Smith GL, Wisloff U. The effect of exercise training on transverse tubules in normal, remodeled, and reverse remodeled hearts. *J Cell Physiol.* 2010

13. Lyon AR, MacLeod KT, Zhang Y, Garcia E, Kanda GK, Lab MJ, Korchev YE, Harding SE, Gorelik J. Loss of t-tubules and other changes to surface topography in ventricular myocytes from failing human and rat heart. *Proc Natl Acad Sci U S A.* 2009;106:6854-6859

14. Kaprielian RR, Stevenson S, Rothery SM, Cullen MJ, Severs NJ. Distinct patterns of dystrophin organization in myocyte sarcolemma and transverse tubules of normal and diseased human myocardium. *Circulation.* 2000;101:2586-2594

15. Kostin S, Scholz D, Shimada T, Maeno Y, Mollnau H, Hein S, Schaper J. The internal and external protein scaffold of the t-tubular system in cardiomyocytes. *Cell Tissue Res.* 1998;294:449-460

16. Sachs F. Stretched activated channels in the heart. In: Kohl P, Sachs F, Franz MR, eds. *Cardiac mechano-electric feedback and arrythmias from pipette to patient.* Philadelphia, PA: Elsevier Saunders; 2005:2-9.

17. Christe G. Localization of K(+) channels in the tubules of cardiomyocytes as suggested by the parallel decay of membrane capacitance, Ik(1) and Ik(atp) during culture and by delayed Ik(1) response to barium. *J Mol Cell Cardiol.* 1999;31:2207-2213

18. Pasek M, Brette F, Nelson A, Pearce C, Qaiser A, Christe G, Orchard CH. Quantification of t-tubule area and protein distribution in rat cardiac ventricular myocytes. *Prog Biophys Mol Biol.* 2008;96:244-257

19. Kohl P, Cooper PJ, Holloway H. Effects of acute ventricular volume manipulation on in situ cardiomyocyte cell membrane configuration. *Prog Biophys Mol Biol.* 2003;82:221-227

20. Mills RW, Narayan SM, McCulloch AD. Mechanisms of conduction slowing during myocardial stretch by ventricular volume loading in the rabbit. *Am J Physiol Heart Circ Physiol.* 2008;295:H1270-H1278

21. McNary TG, Sachse FB. Modeling effects of strain-modulated membrane capacitance and conductance of K+ inward rectifier on conduction velocity in cardiac tissue. *Computing in Cardiology.* 2009:381-384

22. Gonzalez RC, Woods RE. *Digital image processing.* Reading, MA: Addison-Wesley; 1992.

23. Bub G, Camelliti P, Bollensdorff C, Stuckey DJ, Picton G, Burton RA, Clarke K, Kohl P. Measurement and analysis of sarcomere length in rat cardiomyocytes in situ and in vitro. *Am J Physiol Heart Circ Physiol.* 2010;298:H1616-1625

24. Zaniboni M, Cacciani F, Groppi M. Effect of input resistance voltage-dependency on dc estimate of membrane capacitance in cardiac myocytes. *Biophys J.* 2005;89:2170-2181

25. Launikonis BS, Stephenson DG. Tubular system volume changes in twitch fibres from toad and rat skeletal muscle assessed by confocal microscopy. *J Physiol.* 2002;538:607-618

26. Fozzard HA. Membrane capacity of the cardiac purkinje fibre. *J Physiol.* 1966;182:255-267

27. Isenberg G, Kazanski V, Kondratev D, Gallitelli MF, Kiseleva I, Kamkin A. Differential effects of stretch and compression on membrane currents and [Na+]c in ventricular myocytes. *Prog Biophys Mol Biol*. 2003;82:43-56

28. Dyachenko V, Husse B, Rueckschloss U, Isenberg G. Mechanical deformation of ventricular myocytes modulates both TRPC6 and Kir2.3 channels. *Cell Calcium*. 2009;45:38-54

29. Bers DM. Cardiac excitation-contraction coupling. *Nature*. 2002;415:198-205

30. Rizzuto R, Pinton P, Ferrari D, Chami M, Szabadkai G, Magalhaes PJ, Di Virgilio F, Pozzan T. Calcium and apoptosis: Facts and hypotheses. *Oncogene*. 2003;22:8619-8627

31. Crow MT, Mani K, Nam YJ, Kitsis RN. The mitochondrial death pathway and cardiac myocyte apoptosis. *Circ Res*. 2004;95:957-970

32. Matlib MA, Zhou Z, Knight S, Ahmed S, Choi KM, Krause-Bauer J, Phillips R, Altschuld R, Katsube Y, Sperelakis N, Bers DM. Oxygen-bridged dinuclear ruthenium amine complex specifically inhibits Ca2+ uptake into mitochondria in vitro and in situ in single cardiac myocytes. *J Biol Chem*. 1998;273:10223-10231

33. Nutt LK, Pataer A, Pahler J, Fang B, Roth J, McConkey DJ, Swisher SG. Bax and Bak promote apoptosis by modulating endoplasmic reticular and mitochondrial Ca2+ stores. *J Biol Chem*. 2002;277:9219-9225

5. CONCLUSION

The presented studies contribute to our knowledge of structural and functional changes that occur in the heart due to mechanical deformation. The studies were carried out at subcellular, cellular and tissue level. The studies were primarily experimental, but in one case were complemented with a computational study.

The research reported in the second chapter describes biphasic changes in conduction velocity, with a positive strain-velocity relationship for small to midlevel strains and conduction block for large strain. The treatment of the papillary muscles with streptomycin sulfate had a peak conduction velocity at a higher strain before block, which indicates that nonselective stretch activated ion channels are affecting conduction velocity. The streptomycin however had no effect on conduction block indicating other mechanisms are involved in this phenomenon. There was typically a delay of two minutes between adjustment of strain and the electrical measurements, conduction block and recovery from block occurred instantaneously for this temporal discretization. This indicates that no irreversible damage occurred when conduction block was induced. The mechanism of block and the rate of onset with increased strain are unknown.

Besides the limitation of temporal and spatial resolution in the experimental data, the modeling data were limited to qualitatively describe the changes found experimentally. One of the components that contributed to this was the use of a guinea pig ventricular model, which was used to describe the changes in conduction velocity. Though the species difference may be noticeable this change is reasonable because the

electrophysiology in guinea pig myocytes is similar to that in rabbit myocytes with regard to action potential propagation.

The orientation of myocytes in papillary muscle is in the same direction as the muscle, which simplifies the analysis of measured data while complicating the application of results to whole heart studies. This is due to heterogeneity of myocyte orientation of the heart, for instance from epicardial to endocardial tissue and from base to apex. Up until now, it has been assumed that the mechanism causing commotio cordis has only been due to activation of stretch activated ion channels[1]. A study done in atria, though, has shown that conduction block occurs when excessive pressure is applied to atria[2]. Thus, a study covering the effects of increased ventricular pressure to the point of conduction block may be informative.

The second and third chapters described the effects of strain on the t-system, in particular, that the length of t-tubules increases with contraction and decreases with strain. The dynamic nature of t-tubule geometry was not characterized previously. Another feature of t-tubule geometry that was previously not considered is the cross-sectional orientation, which changed from rest to either strain or contraction in the same manner. These dynamic changes in t-tubular geometry suggest a pumping mechanism of the extracellular fluid into (and out of) the lumen of the t-tubular space.

Confocal microscopy was the modality used to measure the features described above. Due to the resolution limit of confocal microscopy the minimum resolving distance between two points was 0.28 μm in the x-y plane. This limitation was exacerbated in the direction parallel to the laser, increasing the minimum resolving distance between two points to 0.83 μm in the z direction[3]. This would not affect the results of Chapters 3 or 4,

though, because t-tubules shorter than 1 μm were not included in the analyses and the average t-tubule diameter in rabbit ventricular cells is 0.45 ± 0.17 μm^3.

The studies in Chapters 3 and 4 suggest changes in membrane tension during these changes in length, which leads to a number of interesting questions, like: "Does tension of the t-system membrane increase during contraction or during strain?" To phrase this question another way: "Is the membrane in a t-tubule anchored to specific regions of the t-tubule environment, or does it extend out into the outer sarcolemmal space during strain?" If the sarcolemma extends into the outer sarcolemmal space with strain, then it may be assumed that the largest strain is at the mouth of the t-tubules. Presuming non-selective stretch activated ion channels are located in functionally relevant positions, then immunolabeling of these channels should indicate increased densities near the mouth of the t-tubules.

The presented studies provide insights in effect of strain on cellular capacitance. Direct measurements of capacitance of ventricular myocytes had not been carried out at rest and during strain in previous studies. A previously developed hypothesis is that the membrane folds and extends as the myocyte is strained and this affects the membrane capacitance[4, 5]. However, the membrane capacitance measured in isolated myocytes did not show changes when strains were applied. This may not discount the possibility that folds in the membrane exist as oscillations in the membrane, which allow for changes in cellular length without changing the capacitance. It may be possible that larger strains (closer to 20%) are needed to induce changes in membrane capacitance. Thus, further experiments are needed to either validate or disprove these possibilities. Higher

resolution imaging may be performed using EM tomography to image the three-dimensional structure of t-tubules and the outer sarcolemma.

Considering the unexpected increase in membrane resistance, with increasing pressure and strain, it is appropriate that we change the hypothesis from the second chapter. The changes reflect what other investigators found using local strain application to single myocytes[6, 7]. Specifically they found inward rectifying potassium channels close with applied strain as the stretch activated ion channels open (Fig. 5.1). Closing of the

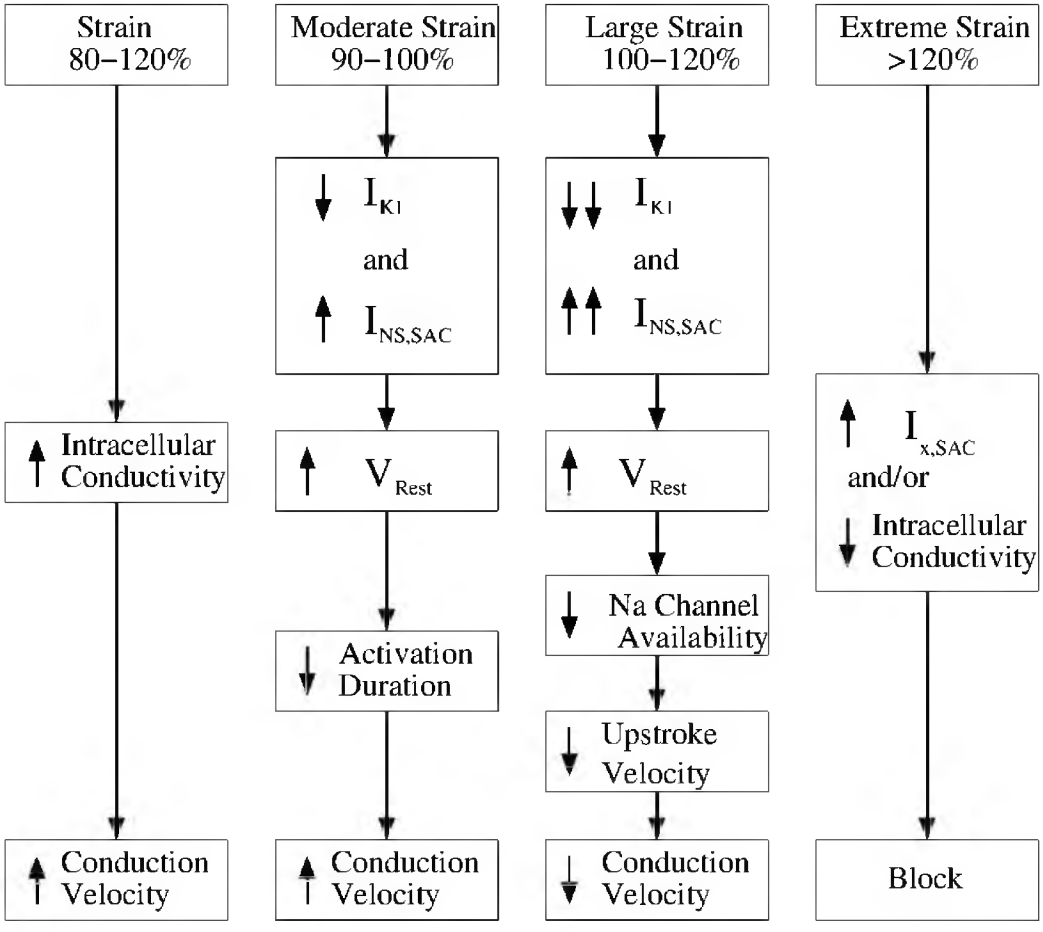

Figure 5.1: Modified hypotheses based on measured changes in membrane resistance. We suggest that three mechanisms play a role in strain-modulated conduction velocity, namely intracellular conductivity, strain sensitive potassium channels, and stretch activated ion channels. The mechanism causing block is unknown, but may be due to hyper- or de-polarization caused by stretch sensitive channels. Gap junction conductance may also change, contributing to conduction block.

inward rectifying potassium channels will reduce the amount of current needed to depolarize the cell, while opening of the stretch activated channels provides the depolarizing current. We hypothesize that the closing and opening of potassium and stretch activated channels, respectively, depend on the channel sensitivity to strain or membrane tension. The cause of conduction block remains unknown, because block occurred at the equivalent of 30% strain in myocytes. Thus, the results from Chapter 4 cannot reliably be applied to explain this phenomenon.

The protocols developed for the described experiments and the findings from these experiments may contribute to understanding the physiology of heart, which is essential to properly understand the pathophysiology. Without knowing the basic physiological mechanisms in the healthy heart we cannot determine how alteration cause heart failure. These presented findings might also be useful in improving models of the function of the heart in silico, which allow us to test hypotheses that cannot be studied directly in experiments.

References

1. Link MS, Maron BJ, Estes NAM. Ventricular fibrillation secondary to nonpenetrating chest wall impact (commotio cordis). In: Kohl P, Franz MR, Sachs F, eds. *Cardiac mechano-electric feedback and arrhythmias.* Philadelphia, PA: Elsevier Saunders; 2005:137-144.

2. Eijsbouts SC, Majidi M, van Zandvoort M, Allessie MA. Effects of acute atrial dilation on heterogeneity in conduction in the isolated rabbit heart. *J Cardiovasc Electrophysiol*. 2003;14:269-278

3. Savio-Galimberti E, Frank J, Inoue M, Goldhaber JI, Cannell MB, Bridge JH, Sachse FB. Novel features of the rabbit transverse tubular system revealed by quantitative analysis of three-dimensional reconstructions from confocal images. *Biophys J*. 2008;95:2053-2062

4. Mills RW, Narayan SM, McCulloch AD. Mechanisms of conduction slowing during myocardial stretch by ventricular volume loading in the rabbit. *Am J Physiol Heart Circ Physiol*. 2008;295:H1270-H1278

5. Kohl P, Cooper PJ, Holloway H. Effects of acute ventricular volume manipulation on in situ cardiomyocyte cell membrane configuration. *Prog Biophys Mol Biol*. 2003;82:221-227

6. Isenberg G, Kazanski V, Kondratev D, Gallitelli MF, Kiseleva I, Kamkin A. Differential effects of stretch and compression on membrane currents and [Na+]c in ventricular myocytes. *Prog Biophys Mol Biol*. 2003;82:43-56

7. Dyachenko V, Husse B, Rueckschloss U, Isenberg G. Mechanical deformation of ventricular myocytes modulates both TRPC6 and Kir2.3 channels. *Cell Calcium*. 2009;45:38-54